HHS Public Access

Author manuscript

Nat Cell Biol. Author manuscript; available in PMC 2022 September 14.

Published in final edited form as:

Nat Cell Biol. 2022 March ; 24(3): 307–315. doi:10.1038/s41556-022-00856-5.

Leucyl-tRNA synthetase is a tumour suppressor in breast cancer and regulates codon-dependent translation dynamics

Maria C. Passarelli[1], **Alexandra M. Pinzaru**[1], **Hosseinali Asgharian**[2,3,4], **Maria V. Liberti**[1], **Søren Heissel**[5], **Henrik Molina**[5], **Hani Goodarzi**[2,3,4,*], **Sohail F. Tavazoie**[1,*]

[1]Laboratory of Systems Cancer Biology, The Rockefeller University, New York, NY, 10065, USA

[2]Department of Biochemistry and Biophysics, University of California, San Francisco, San Francisco, CA 94158, USA

[3]Urology, University of California, San Francisco, San Francisco, CA 94158, USA

[4]Helen Diller Family Comprehensive Cancer Center, University of California, San Francisco, San Francisco, CA 94158, USA

[5]Proteomics Resource Center, The Rockefeller University, New York, NY 10065, USA

Abstract

Tumourigenesis and cancer progression require enhanced global protein translation[1–3]. Such enhanced translation is caused by oncogenic and tumour suppressive events that drive the synthesis and activity of translational machinery[4,5]. Here we report the surprising observation that leucyl-tRNA synthetase (LARS) becomes repressed during mammary cell transformation and in human breast cancer. Monoallelic genetic deletion of LARS in mouse mammary glands enhanced breast cancer tumour formation and proliferation. LARS repression reduced the abundance of select leucine tRNA isoacceptors, leading to impaired leucine codon-dependent translation of growth suppressive genes including epithelial membrane protein 3 (EMP3) and gamma-

Lead and corresponding author: Sohail F. Tavazoie, Leon Hess Professor, Head, Laboratory of Systems Cancer Biology, The Rockefeller University, Box 16,1230 York Avenue, New York, NY 10065 USA, Phone: 212-327-7208 Fax: 212-327-7209, stavazoie@mail.rockefeller.edu.

*These authors jointly supervised this work:

AUTHOR CONTRIBUTIONS

M.C.P and S.F.T. designed the experiments. M.C.P., A.P., M.V.L, S.H. and H.M. performed the experiments. H.G. and H.A. performed ribosome profiling and polysome profiling sequencing analyses. M.C.P. and S.F.T. wrote the paper with input from the co-authors.

COMPETING INTERESTS STATEMENT

S.F.T. is a cofounder, shareholder and member of the scientific advisory board of Inspirna. The remaining authors declare no competing interests.

DATA AVAILABILITY

The data that support the findings of this study have been deposited in the Gene Expression Omnibus (GE) under the accession code GSE176130.

Mass spectrometry proteomics data have been deposited to the ProteomeXchange Consortium via the PRIDE partner repository with the dataset identifier PXD026609.

The human breast cancer data were derived from the TCGA Research Network: http://cancergenome.nih.gov/. The dataset derived from this resource that supports the findings of this study is available from UCSC Xena.

All other data supporting the findings of this study are available from the corresponding author on reasonable request.

CODE AVAILABILITY

Code generated is available from the authors upon reasonable request.

glutamyltransferase 5 (GGT5). Our findings uncover a tumour suppressive tRNA synthetase and reveal that dynamic repression of a specific tRNA synthetase—along with its downstream cognate tRNAs—elicits a downstream codon-biased translational gene network response that enhances breast tumour formation and growth.

To initiate and progress, cancers must establish transcriptomic and proteomic expression programs that enable subversion of host responses[1–3]. A defining feature of such malignant expression programs is enhanced global translation, which has been shown to promote transformation and cancer progression[4,5]. Translation is mediated by ribosomes, which employ aminoacylated transfer RNAs (tRNAs) to decode messenger RNA (mRNA) transcripts. Aminoacyl tRNA synthetases 'charge' tRNAs by covalently ligating each amino acid to cognate isoacceptor tRNAs[6]. Consistent with a positive role for translation in tumourigenesis and cancer progression, specific amino acids[4,7] and tRNAs[8–11] have been shown to be limiting for cancer progression. Recent studies have also demonstrated tumourigenic roles for tRNA synthetases[12] and have revealed dysregulated tRNA synthetase expression in additional diseases[13–15]. By surveying the expression of tRNA synthetases in breast cancer, we observed that leucyl-tRNA synthetase (LARS), an aminoacyl tRNA synthetase that ligates leucine to corresponding leucyl-tRNAs, becomes unexpectedly repressed during breast malignant transformation. Monoallelic genetic deletion of *Lars* in the mammary gland enhanced proliferation and tumour formation in a genetically initiated mouse cancer model. We herein describe our identification and molecular characterization of this unexpected tumour suppressive tRNA synthetase/tRNA gene network.

To identify candidate tRNA synthetases that may play a role in breast tumourigenesis, we assessed the expression levels of all tRNA synthetases in human breast cancers relative to normal breast tissue samples in The Cancer Genome Atlas (TCGA). Surprisingly, while 16/20 tRNA synthetases were overexpressed, LARS, KARS, QARS and DARS were reduced in tumours relative to normal breast tissues (Fig. 1a). We next performed Real-Time Quantitative Reverse Transcription PCR (qRT-PCR) for all tRNA synthetases in the non-transformed human mammary epithelial cell line MCF10A compared to the breast cancer HCC1806 cell line (Extended Data Fig. 1a). Of the tRNA synthetases reduced by greater than 50%, only QARS and LARS were depleted in both human cell line and TCGA analyses.

To determine if LARS and QARS repression occurs during breast tumourigenesis, we transformed MCF10A cells and the murine mammary epithelial cell line NMuMG by overexpressing the polyoma middle-T (PyMT) oncogene in the context of p53 inhibition by pifithrin-α (PFT)[16]. PyMT-transformed cells successfully formed colonies in soft agar compared to control cells, a hallmark of successful malignant transformation, and PyMT-transformed NMuMG cells formed tumours as early as 14 days post mammary fat pad transplantation in mice (Extended Data Fig. 1b,c). Importantly, 5 days following transformation, we observed a significant reduction in LARS protein levels (Fig. 1b-d). In comparison, QARS was not depleted (Extended Data Fig. 1d,e), nor were other aaRS including isoleucyl, histidyl and asparaginyl -tRNA synthetases (IARS, HARS, NARS,

respectively) (Extended Data Fig. 1f,g). These data reveal that LARS specifically becomes repressed during malignant transformation of mammary epithelial cells.

To assess the generalizability of LARS depletion in breast cancer, we assessed LARS expression levels across multiple human and mouse cell lines. Copy number assays in MCF10A and HCC1806 cells suggested a loss of LARS at the genomic level (Extended Data Fig. 1h). In addition, LARS mRNA and protein expression were lower in MDA-MB-231, HCC1806 and T47D breast cancer cell lines relative to non-transformed MCF10A cells (Fig. 1e,f, Extended Data Fig. 1i). Similarly, LARS mRNA and protein levels were reduced in murine breast cancer lines 4T07 and EO771 relative to non-transformed NMuMG cells (Fig. 1e, 1g, Extended Data Fig. 1j). We did not observe further reduced expression of LARS in highly metastatic cells relative to poorly metastatic cells when analyzing either human (MDA-MB-231 parental versus the MDA-LM2 highly metastatic derivative) or murine (67NR and 4T07 poorly metastatic versus 4T1 highly metastatic) isogenic lines, suggesting that LARS repression may regulate breast cancer formation rather than metastatic progression (Extended Data Fig. 1k,l).

To determine if LARS directly regulates tumourigenesis, we utilized the established MMTV-PyMT genetically initiated murine model of breast cancer[17]. PyMT animals expressing MMTV-driven *Cre*-recombinase were crossed to animals homozygous for a *Lars* allele harboring loxP sites[18], enabling constitutive monoallelic deletion of *Lars* in the mammary epithelium. As expected, monoallelic deletion reduced LARS protein levels by ~50% (Fig. 2a,b). Remarkably, LARS depletion was sufficient to significantly increase the number of palpable tumours at 12 weeks of age, a typical tumour initiation time point in this model[17,19] (Fig. 2c). LARS depletion also substantially increased primary tumour burden (Fig. 2d). Immunofluorescence staining of tumour sections with the proliferation marker Ki67 revealed enhanced proliferation in *Cre*-positive $Lars^{fl/+}$ animals compared to *Cre*-negative littermates (Extended Data Fig. 2a,b). To assess whether LARS-dependent tumour growth effects observed *in vivo* were cell autonomous, we derived heterotypic organoids from PyMT tumours of *Cre*-positive and *Cre*-negative $Lars^{fl/+}$ mice[20]. When cultured in Matrigel, *Cre*-positive $Lars^{fl/+}$ organoids exhibited significantly increased growth relative to *Cre*-negative organoids (Fig. 2e,f). Moreover, these growth changes were rescued by wild-type LARS re-expression in *Cre*-positive organoids, but not by expression of previously characterized LARS mutants lacking leucine-binding capacity (F50A/Y52A) or catalytic site activity (K716A/K719A)[21,22] (Extended Data Fig. 2c,d). Conversely, overexpression of wild-type LARS, but not mutant LARS, in wild-type PyMT organoids reduced growth (Extended Data Fig. 2e,f). These findings identify LARS as a tumor suppressor in breast cancer through repression of mammary tumour initiation and cell-autonomous growth.

LARS ligates leucine amino acid to all five tRNA-Leu isoacceptors. Given that LARS-mediated growth changes could be rescued by wild-type but not catalytically inactive LARS overexpression, we reasoned that LARS-dependent tumour suppression may occur through altered charging levels of specific leucyl-tRNAs. To test this hypothesis, we adapted our previously reported tRNA capture-sequencing profiling approach[8] to allow for relative quantification of charged tRNA species, in charged tRNA profiling. In brief, we isolated RNA under acidic conditions to preserve aminoacyl-tRNA bonds and then oxidized

uncharged tRNAs with sodium periodate ($NaIO_4$)[23–25], leaving only charged species available for downstream biotinylation and capture for sequencing as previously described. In parallel, total tRNA was isolated for comparison (Fig. 3a). Given the previously observed differences in LARS protein expression, we performed charged tRNA profiling in HCC1806 cells compared to MCF10A cells. Our data revealed reduced amino acid charging of four out of five leucyl tRNA isoacceptors in HCC1806 cells relative to MCF10A cells (Fig. 3b). Among these tRNAs, tRNA-Leu^{CAG} exhibited the greatest magnitude of reduction. Of note, the same tRNA-Leu species were reduced in total tRNA quantification, with tRNA-Leu^{CAG} exhibiting the greatest effect (Extended Data Fig. 3a). These findings are consistent with the literature, whereby uncharged tRNAs are less stable than charged tRNAs, causing a reduction in overall tRNA abundance[26,27]. Moreover, northern blot analysis for the most significantly depleted tRNA-Leu species—tRNA-Leu^{CAG}, tRNA-Leu^{AAG}, and tRNA-Leu^{UAG}—confirmed a reduction in overall expression of these tRNAs in HCC1806 relative to MCF10A cells (Fig. 3c). The levels of these tRNAs were also reduced in LARS-depleted 4T07 cells (Extended Data Fig. 3b-d). We also examined charged tRNA levels in LARS-depleted 4T07 cells by acid urea PAGE. Using this approach, we observed a reduction in charged to total tRNA ratio in LARS-depleted cells compared to control (Extended Data Fig. 3e-f). Taken together, these results indicate that LARS depletion reduces the overall abundance of charged and total tRNA-Leu^{CAG}, tRNA-Leu^{AAG}, and tRNA-Leu^{UAG}.

We next asked whether tumour suppression by LARS may be mediated by specific leucyl tRNAs. We employed CRISPRi[28] to repress transcription of the most significantly reduced leucyl tRNA, tRNA-Leu^{CAG}, and assessed the impact of this on mammary epithelial cell transformation (Extended Data Fig. 3g,h). Remarkably, CRISPRi-mediated depletion of tRNA-Leu^{CAG} in MCF10A cells enhanced PyMT-induced colony formation by soft agar assay (Fig. 3d). These findings identify tRNA-Leu^{CAG} as a mammary tumour suppressor downstream of LARS.

To determine whether LARS repression could enhance tumorigenesis through altered tumoral leucine availability, we conducted mass spectrometry-based metabolite profiling of branched chain amino acids within 4T07 LARS-depleted tumour cells implanted into mice. Intratumoural levels of leucine, isoleucine and valine were not significantly altered in LARS-depleted relative to control tumours (Extended Data Fig. 3i-k). This finding suggests that LARS depletion does not meaningfully impact tumoural abundance of leucine or of other branched-chain amino acids in this model.

To further characterize the impact of LARS depletion on translation dynamics, we employed multiple translation profiling approaches. First, we conducted polysome profiling in 4T07 LARS-depleted cells. Polysome fractions were pooled into low-translated (1–2 ribosomes) and high-translated (>3 ribosomes) groups and associated mRNA transcripts were sequenced (Extended Data Fig. 4a). We reasoned that if LARS repression promotes tumourigenesis through reduced leucyl tRNA availability, we would expect leucine-rich transcripts to exhibit decreased polyribosome association. To test this hypothesis, we calculated differential gene expression in high-translated versus low-translated groups, in LARS-depleted samples compared to control. We binned differentially expressed transcripts into four quartiles based on total leucine codon content, and plotted the $\log_2$ fold changes as a cumulative

distribution function (Fig. 4a). Transcripts with the most leucine codons (top 25%) exhibited a significant left shift in $\log_2$ fold change compared to transcripts with the fewest codons (bottom 25%), consistent with a reduction in leucine-rich translation upon LARS depletion. The analysis was repeated, instead ranking and binning transcripts by leucine isoacceptor content. Top quartiles of Leu-CUC and Leu-CUG codon enriched transcripts also exhibited a significant left shift in $\log_2$ fold change, whereas other Leu codons demonstrated no difference or a right shift in $\log_2$ fold change (Fig. 4b,c, Extended Data Fig. 4b-e). These data suggest that LARS impacts protein translation in a codon-dependent manner, first affecting Leu-CUC and Leu-CUG enriched transcripts, which account for ~60% of leucine incorporation into proteins[29,30]. Notably, Leu-CUG is decoded by tRNA-Leu^{CAG}, which was observed to repress transformation as described above, while Leu-CUC contains a wobble position and would be decoded by inosine-modified tRNA-Leu^{AAG} [31]. As an orthogonal *in vivo* approach, we employed the RiboTag model[19,32] within our *Lars*-depleted PyMT tumour model to capture tumoral ribosome-associated mRNAs. Consistent with polysome profiling findings, differentially expressed leucine-rich genes in *Lars*$^{fl/wt}$ compared to wild-type tumours revealed a significant left-shift in cumulative distribution of $\log_2$ fold change (Extended Data Fig. 4f-h). These effects were more modest because the RiboTag system does not enrich for polysomes relative to monosomes. These findings reveal that LARS depletion reduces polysome and ribosome association of leucine enriched transcripts, suggesting that reduced abundance of leucyl tRNAs significantly reduces translation of transcripts enriched in cognate leucyl codons.

To further assess the impact of LARS depletion on leucine-rich protein translation, we conducted RiboSeq[33] on LARS-depleted 4T07 cells. We first calculated translation efficiency for each transcript, as a ratio of ribosome protected fragment occupancy to mRNA abundance. To assess the specific sensitization of Leu-enriched transcripts to LARS reduction, we examined $\log_2$ fold translation efficiency ratios (logTER) in shLARS as a function of fractional CUG codon content (Extended Data Fig. 4i, Supplementary Table 1). We found a significant negative correlation between increased CUG fraction and logTER, consistent with our observation that CUG codon enrichment sensitizes mRNAs to LARS reduction.

We next asked whether ribosome dwell time over each codon differed in LARS-depleted samples compared to control. To assess this, we calculated codon level bias coefficients, a measure proportional to ribosome dwell time. Regression of bias coefficients against cell lines demonstrated an increase in dwell time for all Leu codons in LARS-depleted samples compared to control. Importantly, LARS-mediated dwell time changes were significantly increased for Leu codons compared to other codons (Extended Data Fig. 4j). These data suggest that LARS depletion preferentially enhances ribosome dwell time over leucine codons.

Finally, we asked if local translation rates were affected by clusters of leucine codons within a given gene. We calculated sequence discrepancy for leucine codons across all transcripts in control cells, a value from 0 to 1 where 0 corresponds to an even distribution and 1 is perfectly uneven. We observed a significant positive correlation between sequence discrepancy and bias coefficient, suggesting that ribosome dwell time increases as leucine

clustering increases (Extended Data Fig. 4k). Taken together, these data reveal that LARS depletion significantly impacts translation at leucine codons and reveal increased ribosome dwelling at regions of transcripts enriched in leucine codons.

To identify candidate genes that mediate LARS-dependent tumor suppression, we performed tandem mass tag (TMT)-labeled proteomics[34] on tumours derived from PyMT mice with monoallelic *Lars* deletion. We identified a set of proteins that were significantly repressed in the context of LARS heterozygosity ($p<0.05$, Fig. 4d, Supplementary Table 2). A majority of these candidates were enriched in Leu codons, particularly Leu-CUC or Leu-CUG. We focused on epithelial membrane protein 3 (EMP3) and gamma-glutamyltransferase 5 (GGT5)—two genes that were relatively enriched in Leu-CUC and Leu-CUG codons and whose expression levels were found to be reduced in human breast tumours relative to non-cancerous mammary tissue in TCGA (Extended Data Fig. 5a,b, Supplementary Table 2). Western blot analysis confirmed reduced EMP3 and GGT5 protein levels in LARS-depleted tumours as well as in LARS-depleted NMuMG cells (Fig. 4e,f, Extended Data Fig. 5c-f). Importantly, EMP3 and GGT5 mRNA abundances were not reduced, suggesting that downregulation of these proteins is likely due to LARS-mediated translation changes, not mRNA stability or transcriptional downregulation (Extended Data Fig. 5g-h).

EMP3 is a small transmembrane protein thought to be involved in cell proliferation, and has been implicated in cancer including as a tumor suppressor in certain solid tumours[35,36]. GGT5 is a glutathione metabolism related proenzyme, which has been shown to play a non-cell autonomous role in overcoming chemoresistance in ovarian cancer[37]. To further assess the roles of these proteins in tumour growth, we derived organoids from PyMT tumours and transduced them with shRNAs targeting *Emp3* or *Ggt5*. Following transduction, organoids were cultured in Matrigel and growth changes were assessed. Depletion of either EMP3 or GGT5 enhanced organoid growth (Fig. 5a,b). These findings implicate EMP3 and GGT5 as LARS-regulated tumour suppressors in breast cancer.

Finally, to determine if LARS repression can mediate codon-dependent translation of a downstream target gene, we performed codon-based mutagenesis studies of EMP3. We designed reporter constructs containing EMP3 where LARS-sensitive codons Leu-CUC and Leu-CUG were mutated to the synonymous codon Leu-UUG, a codon for which translation was not significantly impacted upon LARS depletion (Fig. 5c). We observed that the codon mutant form of EMP3 was less repressed by LARS depletion, consistent with direct LARS- and Leu-codon-dependent regulation of EMP3 (Fig. 5d,e). These findings confirm the existence of a direct translational regulatory response downstream of LARS in mammary tumour suppression.

Our work identifies LARS, a specific tRNA synthetase, as a breast tumour suppressor. We show that repression of LARS reduces the charging and function of tRNA-Leu^{CAG} to suppress malignant transformation. Depletion of LARS reduces leucine rich protein translation and expression of candidate tumor suppressors including EMP3 and GGT5 (Fig. 5f). These findings suggest that LARS regulates a tumour suppressive network. Moreover, this work demonstrates that specific repression of a tRNA synthetase can modulate translation of tumour suppressors enriched in a cognate codon.

We observed that LARS downregulation promotes mammary tumour formation. These findings are surprising; translational upregulation is classically thought to be a growth-promoting process, as activation of multiple oncogenes including MYC, AKT and PI3K drives transcription and translation of ribosomal RNA, ribosomal protein genes, and other specific oncogenes[2,4,38]. As such, in the context of global translation upregulation, specific mechanisms are needed to prevent translational enhancement of tumour suppressors. We propose that LARS repression serves such a purpose by repressing translation of specific tumour suppressors enriched in specific leucine codons. The interactions of nutrient stress and amino acid availability with tRNA charging and translation have been investigated[4,7,39–41], as have the roles of specific tRNA synthetases in enhancing cancer phenotypes[12] – including LARS, in the context of lung cancer[42]. Our findings provide evidence in mammalian cells of tRNA synthetase-mediated suppression of translation in a cognate codon-dependent manner, serving a tumour suppressive function in mammary cells.

We noted a reduction in not only charged, but also total tRNA-Leu abundances in our tRNA profiling. This finding is consistent with literature demonstrating that uncharged tRNAs are less stable than their charged counterparts, leading to tRNA degradation[27]. Interestingly, we also observed that LARS reduction preferentially affects charging and expression of tRNA-Leu^{AAG}, tRNA-Leu^{UAG} and tRNA-Leu^{CAG}, over tRNA-Leu^{UAA} and tRNA-Leu^{CAA}. One possible explanation for this may be sequence–and thus structural–differences between these species (Supplementary Table 3) that may affect tRNA binding to the tRNA synthetase[43–47]. Our findings are also consistent with tRNA charging studies in the context of amino acid limitation, whereby leucine limitation preferentially reduced charging of tRNA-Leu^{AAG}, tRNA-Leu^{UAG} and tRNA-Leu^{CAG} over tRNA-Leu^{UAA} and tRNA-Leu^{CAA} [39]. Intriguingly, tRNA-Leu^{AAG}, tRNA-Leu^{UAG} and tRNA-Leu^{CAG} are more common than tRNA-Leu^{UAA} and tRNA-Leu^{CAA}. Interestingly, the role of tRNA synthetases in regulating charged tRNA pools has recently been attributed to reduced ability of tRNA synthetases to bind and sequester uncharged tRNAs[48]. In sum, further research is warranted especially in the context of *in vivo* models to examine the regulatory effects of tRNA synthetases and other factors on tRNA abundance and the maintenance of charged tRNA pools.

Many tRNA synthetases serve cellular functions independent of their role in aminoacylation[49]. In particular, LARS has been identified as a sensor of intracellular leucine in activating mTOR signaling[21]. In our system, rescue experiments with catalytically inactive forms of the protein that abrogate charging failed to rescue the growth phenotypes (Extended Data Fig 2b,c). Given that both mutants failed to rescue growth changes relative to a wild-type rescue, tumor-suppressive tRNA charging changes are likely the dominant phenotype in our system. Nevertheless, the proposal of a pro-growth, noncanonical function for this enzyme contrasts with our current findings and requires further study given the reportedly pleiotropic nature of this enzyme.

While we have identified specific proteins as downstream mediators of LARS-dependent translational regulation of tumourigenesis, we uncovered a larger set of genes that may govern additional phenotypes and processes. Future studies are needed to explore and uncover unanticipated roles for LARS-mediated translation regulation in metabolic and homeostatic regulation. More broadly, our findings motivate systematic studies across

tRNA synthetases as dynamic translational regulators of gene networks subserving various biological processes in health and disease.

METHODS

Ethical regulations

All animal experiments were performed under supervision and approval of the Institutional Animal Care and Use Committee (IACUC) at the Rockefeller University.

Cell Culture

MCF10A cells (ATCC, CRL-10317) were cultured in DMEM/F12 media supplemented with 5% horse serum and final concentrations of 20 ng/ml of EGF, 0.5 μg/ml of hydrocortisone, 100 ng/ml of cholera toxin, and 10 μg/ml of insulin.

EO771 (ATCC, CRL-3461), HCC1806 (ATCC, CRL-2335) and derivative HCC1806-LM2C cells were cultured in RPMI media supplemented with 10% FBS, 1mM glucose, 10 mM HEPES and 1 mM sodium pyruvate. 293T (ATCC, CRL-3216), MDA-MB-231 (ATCC, HTB-26), T47D (ATCC, HTB-133), NMuMG (ATCC, CRL-1636) 4T07, 4T1 and 67NR cells were cultured in DMEM media supplemented with 10% FBS. (4T1: ATCC, CRL-2539, 4T07 and 67NR were a generous gift by W. P. Schiemann) All human cell lines were STR tested and all lines were routinely tested for mycoplasma contamination.

Generation of stable cell lines

Lentivirus was produced in 293T cells grown in 10 cm plates. Cells were transfected with 1.7 μg and 2.6 μg of packaging plasmids pMD2.g and psPAX2 respectively, 3.4 μg of pLKO.puro1 vector containing the appropriate shRNA, using 40 μL Lipofectamine 2000 (Invitrogen). After 24 hours, the media was replaced with fresh media and virus-containing supernatant was harvested 48 and 72 hours after transfection. The supernatant was filtered through a 0.45 μm filter before 1–2 mL of virus was used with 8ug/mL polybrene to transduce pre-plated 4T07 cells at 75% confluence. Following 24 hours of transduction, selection was conducted using 4 μg/mL puromycin. mRNA and protein knockdown were validated by qPCR and western blot, respectively.

Generation of CRISPRi cell lines

sgRNAs targeting specific tRNA loci were designed by identifying all possible guides (PAM sequences) within 200bp of tRNA transcription start sites for a given isodecoder. Appropriate target-specific guides were selected to be unique among an individual tRNA isoacceptor. Target-specific guides cloned into lentiGuidePuro vector (Addgene #52963). Following lentiviral production as described above, individual sgRNAs were transduced into MCF10A cells stably expressing pHR-SFFV-dCas9- BFP-KRAB (Addgene #46911). tRNA depletion was validated by Northern blot in cells subsequently used for experiments.

PyMT Transformation

Mammary epithelial cell lines were seeded to 70% confluence and transduced the following day with lentivirus expressing pH3-PyMT as described above. After 24 hours

of transduction, blasticidin selection was performed for 3 days at 3 μg/mL and cells were treated with 10 μM pifithrin-α (Sigma) for 5 days.

RNA isolation and purification

RNA was extracted from cells with TRIzol reagent (Life Sciences) followed by isopropanol precipitation at −20°C. After centrifugation at maximum speed (~21,000 × g) in a pre-chilled tabletop microcentrifuge, RNA pellet was washed twice with cold 75% ethanol following resuspension in Rnase free water.

Northern Blot

Purified RNA was run on a 10% Urea-PAGE gel before being transferred onto a nylon membrane and UV crosslinked (240 mJ/cm^2). The membrane was pre-hybridized in UltraHyb-Oligo buffer (Ambion) at 42°C. DNA oligos were radiolabeled with [γ−^{32}P] ATP using T4 PNK (NEB) and further purified by G-50 columns before incubating with the blot overnight. After hybridization, the blot was washed twice with SSC and SDS buffers before being developed. Probes that were ^{32}P labeled and used for detection are described in Supplementary Table 4. Quantification was done using FIJI (ImageJ) where the intensity of each band over background was measured and normalized to U6 levels.

Acidic RNA extraction

1 day prior to RNA extraction, LARS-depleted 4T07 cells (or MCF10A, and HCC1806 cells) were plated to be 80% confluent at time of RNA harvest. On the day of harvest, cell pellets were lysed in 600 μl cold lysis buffer (0.3 M NaOAc, pH 4.5, 10 mM EDTA pH 8), and extracted twice with equivalent volume acidic phenol chloroform (pH 4.5, ThermoFisher). Nucleic acids were precipitated twice with 2.5 volumes of ethanol and 2 μl GlycoBlue (Invitrogen) overnight. Precipitations were centrifuged for 20 minutes at maximum speed at 4°C, and nucleic acids were resuspended in 10 μL of 10 mM NaOAc (pH 4.5).

Acid Urea PAGE

Acidic urea PAGE was adapted from previously described protocols[25]. Briefly, acidic RNA was mixed with 1.5X acidic loading dye (8 M Urea, 0.1 M NaOAc/HOAc, pH 4.8, 0.05% Bromophenol blue, 0.05% Xylene cyanol) and run on a 6.5% PAGE sequencing gel (8M Urea, 0.1M NaOAc pH = 4.5). Samples were run for 24 h at 300V at 4 °C, in 0.3M NaOAc (pH 4.5) running buffer. Samples were then transferred onto a nylon membrane using a semi-dry transfer system for 45 minutes at 0.15A, and UV crosslinked (240 mJ/cm^2). The membrane was pre-hybridized in UltraHyb-Oligo buffer (Ambion) at 42°C. and then hybridized using pre-labeled DNA oligos as described above.

Charged tRNA Capture-Sequencing profiling

$NaIO_4$ Oxidation and precipitation—First, acidic RNA was extracted as described above and resuspended in 30 μL of 10mM NaOAc (pH 4.5). To oxidize free 3'OH on uncharged tRNAs, for each sample, 20μg RNA (at concentration 0.1 μg/μL) was treated with 50 mM $NaIO_4$ (or 50 mM NaCl as a control), in the presence of 100mM KOAc

(pH 4.8). Samples were incubated at 22°C for 30 minutes, and 100 mM glucose added to quench the reaction for an additional 5 minutes. To clean up and enrich for tRNAs, samples were filtered through microRNA enrichment columns (microRNA Purification Kit, Norgen Biotek) according to the manufacturer's instructions. Following ethanol precipitation, samples were filtered through a Sephadex G25 column (GE Life Sciences) to remove excess $NaIO_4$ and precipitated twice with ethanol premixed with 0.1x NaOAc (3M, pH 4.5) and 2 μL GlycoBlue.

tRNA profiling—tRNA profiling was conducted as previously described[8]. Briefly, samples were deacylated with 0.1 M Tris-HCl (pH 9) at 37°C for 30 minutes, precipitated, and biotinylated using Pierce RNA 3' End Biotinylation Kit (Thermo Fisher), with 0.66 pmol of yeast tRNA-Phe added as a spike-in standard. Following chloroform extraction, biotinylated RNA was hybridized to DNA probe pairs complementary to the 3' and 5' arms of each tRNA isoacceptor. Nicks at the anticodon loop of DNA-RNA hybrids were ligated using SplintR ligase and T4 DNA ligase (NEB). DNA-RNA hybrids were purified using My-One-C1 Streptavidin Dynabeads (Invitrogen), and ligated probes were eluted after Rnase H and Rnase A treatment. Probes were PCR amplified and sequenced using Illumina NextSeq (MidOutput, 150 SR) at the Rockefeller University Genomics Center. For computational analysis, fastq files were aligned to tRNA probe sequences using bowtie2, and reads were further sorted, indexed, and counts were generated with samtools. Raw counts were imported into R 4.0.2 and differentially expressed transcripts determined using DESeq2.

Quantitative RT-PCR

To measure mRNA transcript levels, RNA was converted to cDNA (SuperScript III, Life Technologies) followed by Fast SYBR™ Green quantification (Life Technologies) according to manufacturer's instructions. Expression levels of mRNA were performed with either an ABI Prism 7900HT Real-Time PCR System (Applied Biosystems) or a QuantStudio 5 Real-Time PCR System (Applied Biosystems). Target-specific primer sequences can be found in Supplementary Table 5.

Colony Formation Assays

600 cells were plated in 24-well plates, (or 3,000 cells in 6-well plates), in 0.6% Noble agar in standard tissue culture media, atop an underlay of 1% Noble ager and 2X cell culture media. Cells were cultured at 37°C for 18 days and colonies were stained with 0.005% crystal violet and visualized on ChemiDoc Chemiluminescence reader. Colonies formed per 600 cells were counted manually.

Copy Number Assays

Genomic DNA was isolated from cell lines using Qiagen DNA Blood & Tissue Kit and used for Copy Number Assays with TaqPath ProAmp Master Mix, according to the manufacturers instructions, Two assays were used for LARS, Hs06041747_cn and Hs05978602_cn, with RnaseP copy number reference assay (Thermo Scientific) as a normalization control.

Polysome Profiling

Polysome profiling was adapted from previously described protocols[50]. Prior to lysis, pre-plated cells at 80% confluence were treated for 5–7 minutes with media containing 100 μg/mL cycloheximide (Alfa Aesar). Plates were washed with PBS, flash frozen in liquid nitrogen and lysed via scraping using polysome lysis buffer (5 mM Tris HCl pH 7.5, 2.5 mM MgCl2, 1.5 mM KCl, 100 μg/mL cycloheximide, 2 mM DTT, 0.5% Triton X-100, 0.5% sodium deoxycholate, 100 units of SUPERase*In Rnase Inhibitor (Invitrogen), and 1x Protease Inhibitors EDTA-free). Nuclei were removed by centrifugation and cleared lysate concentration was measured using the Quant-iT RiboGreen assay (Life Technologies). 10–50% sucrose gradients were mixed using a Biocomp gradient master with the following conditions: Short Cap, 10% - 50% WV Step 1, 1:50 minutes, 80º angle, 21 speed. Gradients with 150ug lysate loaded were spun using SW41 rotor at 38,000 RPM for 2 hours at 4°C, and then fractionated by 16 using a Triax FlowCell Gradient Fractionator according to the manufacturer's instructions. Based on A280 UV peaks, fractions were pooled in highly translated (3+ ribosomes) and lowly translated (1–2 ribosomes) groups. RNA was extracted using Trizol LS (Life sciences) and 1 μg of RNA was used in library preparation using TruSeq RNA Library Prep (Illumina). Libraries were sequenced using Illumina NextSeq (High Output, 75 SR) at the Rockefeller University Genomics Center. For analysis, fastq files were aligned to mouse genome (mm10) using STAR (v2.5.2a) and reads that were aligned to coding sequences were counted using featureCounts. Raw counts were imported into R and differentially expressed transcripts determined using DESeq2.

RiboTag immunoprecipitation and RNA Sequencing

Tumours were extracted from 24-week old animals and RNA from HA-tagged ribosomes was isolated as previously described[19,32]. 500 ng of RNA was used for RNA sequencing library preparation using TruSeq RNA Library Prep (Illumina). Constructed libraries were sequenced using Illumina NextSeq (High Output, 75 SR) at the Rockefeller University Genomics Center. For analysis, fastq files were aligned to mouse genome (mm10) using STAR (v2.5.2a) and reads that were aligned to coding sequences were counted using featureCounts. Raw counts were imported into R 4.0.2 and differentially expressed transcripts determined using DESeq2.

RiboSeq

Cells were washed and flash frozen with liquid nitrogen before lysis with cycloheximide-containing lysis buffer (Alfa Aesar). Ribosome profiling library preparation was conducted as previously described[33], and PCR libraries were sequenced using Illumina Nextseq (High Output, 75 SR) at the Rockefeller University Genomics Center.

Ribosome dwell time and Sequency Discrepancy analysis

For the ribosome footprinting data, reads were first subjected to linker removal and quality trimming (cutadapt v1.17). Reads were then distributed among the samples based on their assigned barcodes using fastx_barcode_splitter (using –eol and –mismatches 1). Reads were then collapsed and UMIs were extracted (2 at the 5' end and 5 at the 3' end) using UMI Tools. The reads were aligned against a reference database of rRNAs and tRNAs to remove

contaminants (using bowtie 2.3.4.1). bowtie2 was used to align remaining reads to a curated transcriptome (build mm10) containing only the longest CDS for each gene whose lengths were multipliers of 3, to assign reads to codons unambiguously. PCR duplicates were removed using UMI Tools. Xtail[51] was used to count RPFs, estimate translation efficiency, and perform statistical comparisons. For RNA-seq data analysis, reads were first subjected to quality trimming and adapter removal. STAR (v2.5.2a) was used to align the reads to the mouse transcriptome (mm10). The number of reads mapping to each gene was counted using htseq-count.

To assess the quality of ribo-seq data, we checked read length distribution and frame periodicity – overall and stratified by read length –using the R package riboWaltz[52]. Reads in the length range of 28:36 were retained. We next calculated P-site offsets and assigned reads to codon positions to determine codon usage.

Ribosome dwell times at specific codons were compared along transcripts with at least 10 reads in all samples. Background translation rate for each transcript was determined as the median of non-zero rpf read counts among the codons after loess smoothing of observed counts. An excess ratio was calculated at each codon position as the ratio of smoothed rpf counts at that position divided by the transcript background. We named the geometric mean of excess ratios across replicates “stalling bias coefficient” – which is proportional to ribosomal dwell time and inversely proportional to codon decoding rate or local translation rate. Then, we compared the relative dwell times at each codon type across cell lines using linear models in R and plotted the results using the jtools package, comparing LARS depleted cells to control cells.

To assess the effect of Leu codons clusters on local translation rates, we used a measure called “sequence discrepancy” implemented in the R package DiceDesign which was developed based on the theory expounded by Hickernell[53]. Sequence discrepancy is in the range [0–1] with values close to 0 corresponding to uniform (even) distribution and values close to 1 indicating strong clustering of points. For each transcript, we calculated sequence discrepancy of Leu residues. Discrepancy indices were $\log_2$ transformed to reduce skewness. We regressed the average dwell time (stalling bias coefficient) of Leu codons of each transcript against its $\log_2$ transformed Leu discrepancy. We also checked for potential confounding effects of transcript length and the total number of Leu residues.

Protein isolation

Pelleted cells were lysed using RIPA buffer (Life Sciences) using HALT protease inhibitor cocktail (Sigma). Genomic DNA was sheared through a 27G needle, followed by centrifugation to clear cellular debris. Cleared protein lysate concentrations were quantified using BCA protein assay kit (Thermo Fisher).

Flash frozen tissue samples of 50–100 mg were isolated over dry ice and lysed using 100–200 μL RIPA buffer with HALT protease inhibitor cocktail. Tissue homogenization was conducted using a microtube homogenizer (Cole-Parmer), followed by centrifugation and quantification of cleared protein lysate as above.

Organoid samples were digested from reduced growth factor Matrigel in 10mM EDTA in PBS for 1 hour at 4°C, After centrifugation and resuspension in 20–40 μL RIPA buffer, protein lysate samples were cleared and quantified as above.

Western Blot

Protein lysates were heated with LDS buffer and reducing agent (Life sciences) before running on an SDS-PAGE gel and transferred to a PVDF membrane (Bio-Rad). Membranes were blocked using 5% BSA or Odyssey blocking buffer (PBS) and then incubated with the following target-specific antibodies: LARS (Cell Signaling, 13868S, 1;1000), HSC70 (B6) (Santa Cruz, sc-7298, 1:3000), PyMT (Novus Biologicals, NB100–2749, 1:2500), EMP3 (Abcam, ab236671, 1:500), GGT5 (GeneTex, GTX81477, 1:500), α-tubulin (Cell Signaling, 3873S, 1:1000), QARS (Proteintech, 12645–1-AP, 1:1000), HARS (Proteintech, 16375–1-AP, 1:1000), NARS (Aviva Systems Biology, OAAB07325, 1:1000), IARS (ThermoFisher, PA5–44246, 1:1000), HA (BioLegend, 901501, 1:1000), Luciferase (Proteintech, 27986–1-AP, 1:1000).

Tandem Mass Tag Proteomics

Flash frozen tissue samples were homogenized and lysed as above in detergent free lysis buffer containing 20 mM Tris-HCl pH 7.4, 100 mM KCl, 1 mM EDTA pH 8, 0.5% NP-40 and cOmplete protease inhibitor (Sigma). 100 μg of lysate was acetone precipitated and dissolved in 100 μl 8 M Urea/50 mM triethyl ammonium bicarbonate/10 mM DTT. Reduced cysteines were alkylated with iodoacetamide (Sigma), proteins were extracted by chloroform/water/methanol precipitation, and then were digested overnight using LysC endopeptidase and trypsin (NEB). Samples were labeled with TMT reagents (ThermoFisher Scientific) dissolved in neat acetonitrile, followed by quenching with 5% hydroxylamine. Label check was conducted to verify labeling efficiency, and samples were pooled and purified using a high-capacity Oasis HLB cartridge. Purified peptides were fractionated using a reversed-phase high pH fractionation spin column (Pierce). Fractions were separated by low-pH reversed-phase nano-flow chromatography across a 120-minute linear gradient and analyzed by SPS-MS3 acquisition using a Fusion Lumos mass spectrometer (Thermo Scientific). Spectra were queried against the Mus musculus proteome using Sequest HT through Proteome Discoverer v. 2.5 (Thermo Scientific). Further statistical processing was performed using Perseus v.1.6.5.0[54].

Animal Studies

All animal work was conducted at the AAALAC-accredited Comparative Bioscience Center at Rockefeller University. Work was performed in accordance with protocols approved by the Institutional Animal Care and Use Committee at The Rockefeller University. All animals were housed and fed using the University's standard husbandry protocols. $Lars^{tm1a(KOMP)Wtsi}$ knockout mice were obtained from KOMP Repository at UC Davis[18]. FlpE animals were obtained from the Michel Nussenszweig laboratory. RPL22 floxed (Ribotag) mice were obtained from the Jackson laboratory[25].

Genetically Initiated Models of Breast Cancer

Within the laboratory, C57BL/6 mice were crossed with MMTV-PyMT[17], MMTV-Cre[55] positive mice for at least 8 generations to maintain over 99% C57BL/6 background. Following FlpE-mediated recombination, animals homozygous for Lars^{tm1a} were crossed to MMTV-Cre/MMTV-PyMT hemizygous mice to generate heterozygous *Lars* deletion in the mammary tumour compartment. Overall tumour burden was measured weekly in female animals using digital calipers beginning at week 12. Tumour volumes were calculated as (smaller diameter)^2 × (larger diameter) × π / 6. In accordance with the IACUC-approved protocol, animals are humanely euthanized at 24 weeks of age, or at first sign of distress from large tumor burden (labored breathing, signs of distress or individual tumor exceeding 1500 mm^3), whichever comes first. Mammary tumours were isolated for histology, organoid generation, and flash frozen for RNA and protein extraction, while lungs were isolated for paraffin fixation, all as described above.

Homozygous RPL22 floxed (Ribotag) mice were crossed to MMTV-PyMT+; MMTV-Cre+; heterozygous Lars knockout mice to generate animals heterozygous for HA-RPL22 in the mammary tumour compartment, either heterozygous deletion of *Lars* or wild-type *Lars* expression. Size-matched tumours were extracted from three pairs of age-matched female littermates at 24 weeks of age for use in RiboTag studies. All genotyping primer sequences and product sizes can be found in Supplementary Table 4.

Tumor formation studies

500,000 NMuMG cells expressing the PyMT oncogene or empty control were injected into the fourth mammary gland of 8–12-week-old age-matched female NSG mice (4–5 mice per group.) Tumor size was measured biweekly.

In vivo metabolite profiling

1,000 4T07 cells expressing control shRNA or shRNA targeting LARS were injected into the fourth mammary gland of 8–10-week-old age-matched female balb/cJ mice (5 mice per group). Tumour size was measured biweekly, animals were euthanized and tumours were harvested after 14 days for metabolomic studies. 10–30 mg flash frozen tissue samples were homogenized in 80% LC-MS grade methanol/water (v/v). Samples were vortexed and centrifuged at maximum speed at 4°C for 10 minutes. Supernatant was transferred to new tubes. Samples were dried to completion using a nitrogen dryer and then reconstituted in 30 µl 2:1:1 LC-MS water:methanol:acetonitrile for Liquid-chromatography coupled to High-Resolution Mass Spectrometry (LC-HRMS). The injection volume for polar metabolite analysis was 5 µl.

Histology

Mouse lung and mammary fat pad samples were prepared by perfusion fixation with 4% paraformaldehyde through the right ventricle and incubated in 4% paraformaldehyde overnight. Samples were dehydrated and stored in 70% ethanol, and paraffin embedded and sectioned in 5 µm slices for staining with hematoxylin and eosin (H&E) and by immunofluorescence as described below.

Immunofluorescence

Paraffin embedded slides were deparaffinized using five-minute washes in xylenes (x2), 100% ethanol, 95%, 80% 70% ethanol, and PBS. Antigen retrieval was conducted for 20 minutes in boiling citrate buffer (pH 6, Sigma). Slides were cooled and then blocked in 5% goat serum (Sigma Aldrich) in PBS with 0.05% Tween-20 for 30 minutes. Primary antibody against Ki-67 (Abcam, ab16667, 1:1000) was diluted in blocking solution and samples were incubated overnight at 4°C. Slides were washed three times with PBS-Tween prior to incubation with fluorescence-conjugated secondary antibody (Invitrogen, 1:200) in blocking solution for 1 hour at room temperature. Following 3 PBS-Tween washes with the final wash containing 5 ug/mL DAPI nuclear stain (Roche), samples were dried and mounted using ProlonGold Antifade (Invitrogen). Fluorescence intensity was measured on a Zeiss inverted LSM 780 laser scanning confocal microscope at the Bioimaging Resource Center at Rockefeller University. Images were analyzed using ImageJ, by calculating mean fluorescence intensity of sample to normalized DAPI signal.

Organoid Generation and Culture

Organoids were isolated from MMTV-PyMT animal tumours as previously described[22]. Briefly, size-matched mammary tumours were isolated and minced with scalpel followed by collagenase digestion at 37°C. Digested tumours were DNase treated, and differential centrifugation cycles were conducted at 170 × g for 4 seconds each to isolate organoids from single cell contaminants. Organoids were counted and resuspended at 100–300 organoids per well in reduced growth factor Matrigel (Corning). Following gel solidification, ß-FGF-containing growth factor media was added to all wells.

Plated organoids were passaged or frozen by mechanical digestion of reduced growth factor Matrigel in 10mM EDTA in PBS for 1 hour at 4°C, followed by centrifugation and resuspension in reduced growth factor Matrigel (passage) or 90% fetal bovine serum with 10% DMSO (freezing).

Organoid Lentiviral Transduction

Small organoids were collected by pulsing to 300 rpm for 3 seconds and collecting organoids within the supernatant. Lentivirus collected from 10 cm plates and concentrated overnight using Lenti-X concentrator (TaKaRa) was used to transduce organoids by either magnetofection using ViroMagR/L reagent (OZ Biosciences) according to the manufacturer's recommendation, or by spinfection in ultra-low attachment 96-well plates with 4ug/ml polybrene at 1500 × *g* for 1 hour. 800 organoids were cultured with 25% of 10-cm plate concentrated virus into either 50 or 125 μL total volume. Following overnight incubation at 37°C, media was refreshed and puromycin selection was conducted 24 hours later at 1 μg/mL for 3 days.

Organoid Growth Assays

250 organoids were plated in reduced factor Matrigel (Corning) in glass-bottom plates (USA Scientific). 2D images were acquired of individual organoids on day 1, 3, 5 and 8 after plating using either a Zeiss CellDiscoverer 7 microscope or a Nikon TiE inverted microscope with Andor Neo sCMOS camera. Images were quantified using ImageJ to

outline individual organoids. Growth was calculated as a ratio of the 2D projected area of individual organoids on Day 5–8 compared to Day 1 area.

Codon Reporter Assays

HA-tagged constructs were synthesized by IDT and cloned into the psiCHECK2 vector (Promega), replacing the synthetic Renilla luciferase gene. A 6x glycine linker was placed between the HA tag and the gene. Constructs included wild-type EMP3 gene or EMP3 gene with sets of 10 Leu CUC and CUG codons mutated to Leu UUG residues. 500,000 NMuMg shLars knockdown cells were seeded overnight for transient transfection in 6-well plates. Transfections were performed using 3 μg DNA and 9 μL Lipofectamine 2000 per well (Invitrogen). Cells were harvested 48 hours post transfection for analysis of reporter expression levels by quantitative western blot.

Statistics & Reproducibility

No statistical methods were used to predetermine sample size. No data were excluded from analyses. Allocation to different experiments was randomized, with age- and gender-matching for in vivo experiments. Investigators were not blinded to allocation during experiments and outcome assessment, except during colony formation assay counting.

Extended Data

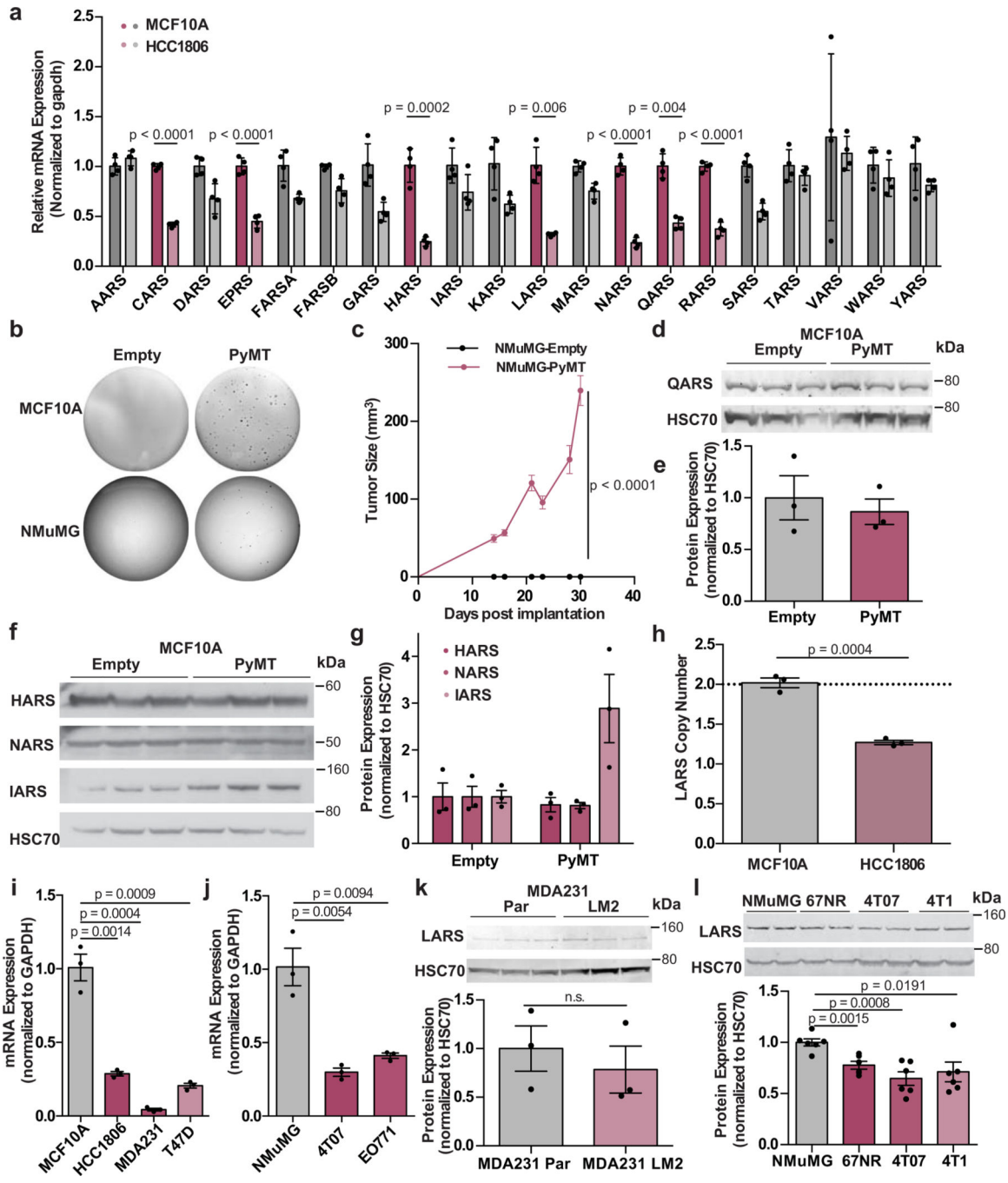

Extended Data Fig. 1. LARS is repressed during malignant transformation.

a, Aminoacyl tRNA synthetase mRNA levels in non-transformed human mammary epithelial cell line MCF10A (left, dark gray or magenta) compared to HCC1806 (right, light gray or pink), normalized to GAPDH. Magenta and pink-colored expression pairs indicate a significant decrease in aaRS expression between MCF10A and HCC1806 of 50% or greater (statistics calculated by unpaired two-tailed Student's t-test with Bonferroni

correction for multiple comparisons, n=4 samples per group). b, Soft agar colony formation assays of PyMT-transformed MCF10A and NMuMG cells compared to empty-transduced control. Representative of n=3 experiments. c, Tumor growth curves for transplanted PyMT transformed NMuMG cells compared to control, statistics calculated by 2-way ANOVA. (n=4 mice per group) d, Western blot of QARS in PyMT-transformed MCF10A cells compared to empty control. e, Quantification of d. f, Western blot of HARS, NARS, IARS in PyMT-transformed MCF10A cells compared to empty control. g, Quantification of f. d-g, HSC70 as a loading control, representative of n=2 independent experiments. h, Genomic copy number assay for LARS in MCF10A and HCC1806 cells, using RNAseP as a normalization control. i, qRT-PCR of LARS mRNA levels in MCF10A, HCC1806, MDA-MB-231 and T47D cell lines, normalized to GAPDH. j, LARS mRNA levels in NMuMG, 4T07 and EO771 cell lines, normalized to GAPDH. k, Above, Western blot of LARS in MDA-MB-231 parental cells compared to highly metastatic LM2 cell lines. Below, quantification. l, Above, Western blot of LARS in NMuMG cell lines compared to isogenic low and high metastatic cell lines 67NR, 4T07 and 4T1. Below, quantification. HSC70 is used as a loading control in i-j. h-l Representative of n=3 independent experiments. All data are mean ± s.e.m., statistics calculated by unpaired two-tailed Student’s t-test.

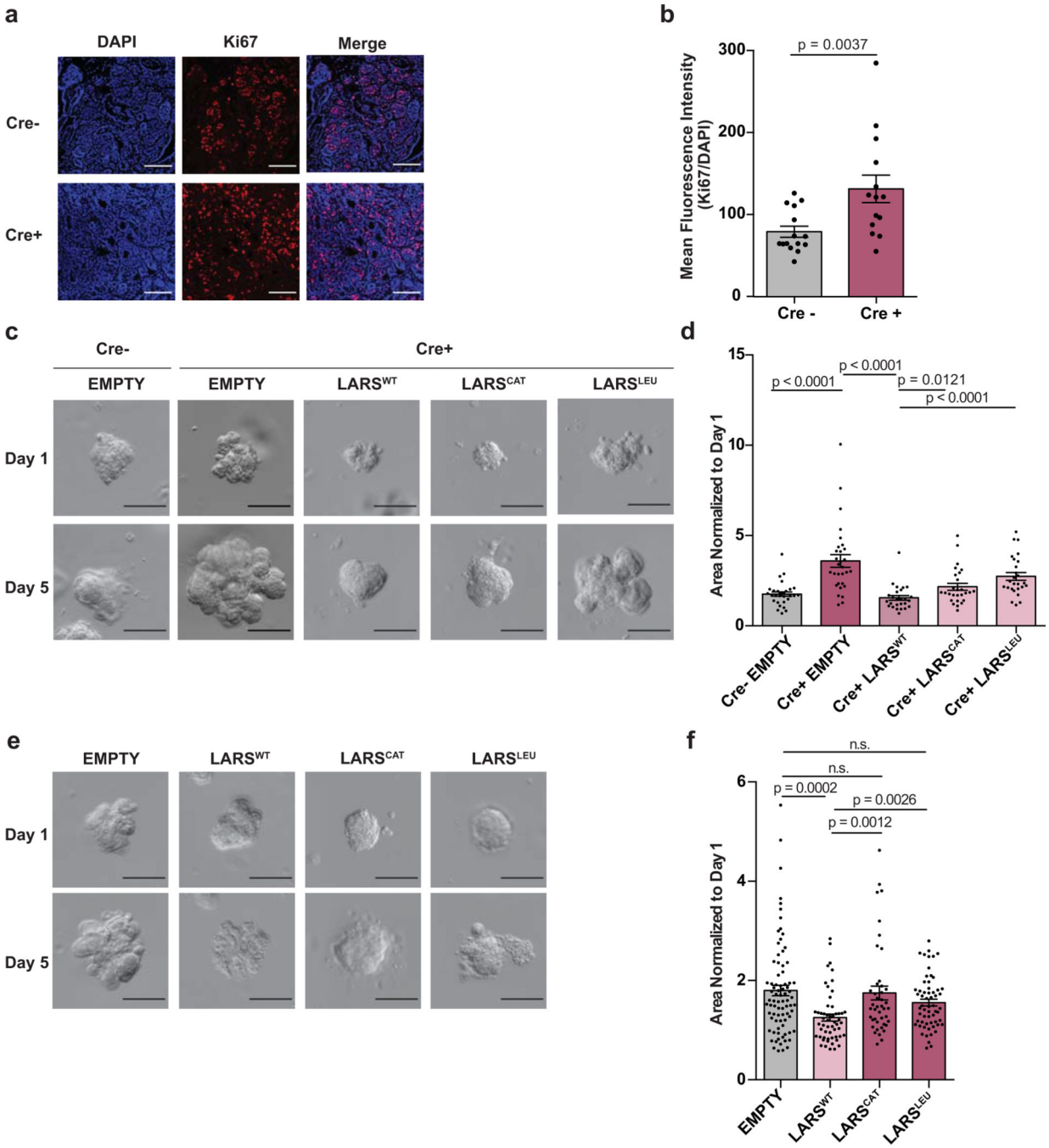

Extended Data Fig. 2. LARS depletion promotes tumor growth.

a, Representative images of Ki-67 staining in LARS-depleted PyMT tumours. Scale bar, 100px. b, quantification of a as mean fluorescence intensity of Ki-67 normalized to DAPI. Cre- n=15, Cre+ n=14, where each data point represents staining from an individual animal. Statistics calculated by two-tailed Mann-Whitney test. c, Representative images of LARS-depleted PyMT Cre+ or Cre- tumour-derived organoids cultured in Matrigel, transfected with LARS constructs – wild-type, catalytically inactive (K716A/K719A) “CAT”, leucine-binding null (F50A/Y52A) “LEU”21,22 or empty vector control. d, Quantification of change

in 2D projection of organoid area, normalized to Day 1. 26–30 organoids quantified per experimental group, representative of n=3 independent experiments e, Representative images of wild-type PyMT tumour-derived organoids cultured in Matrigel, transfected with indicated LARS constructs. f, Quantification of change in 2D projection of organoid area, normalized to Day 1. 44–81 organoids quantified per experimental group, representative of n=3 experiments c-f, Scale bar, 100 μm, Statistics calculated by unpaired two-tailed Student's t-test. All data are mean ± s.e.m.

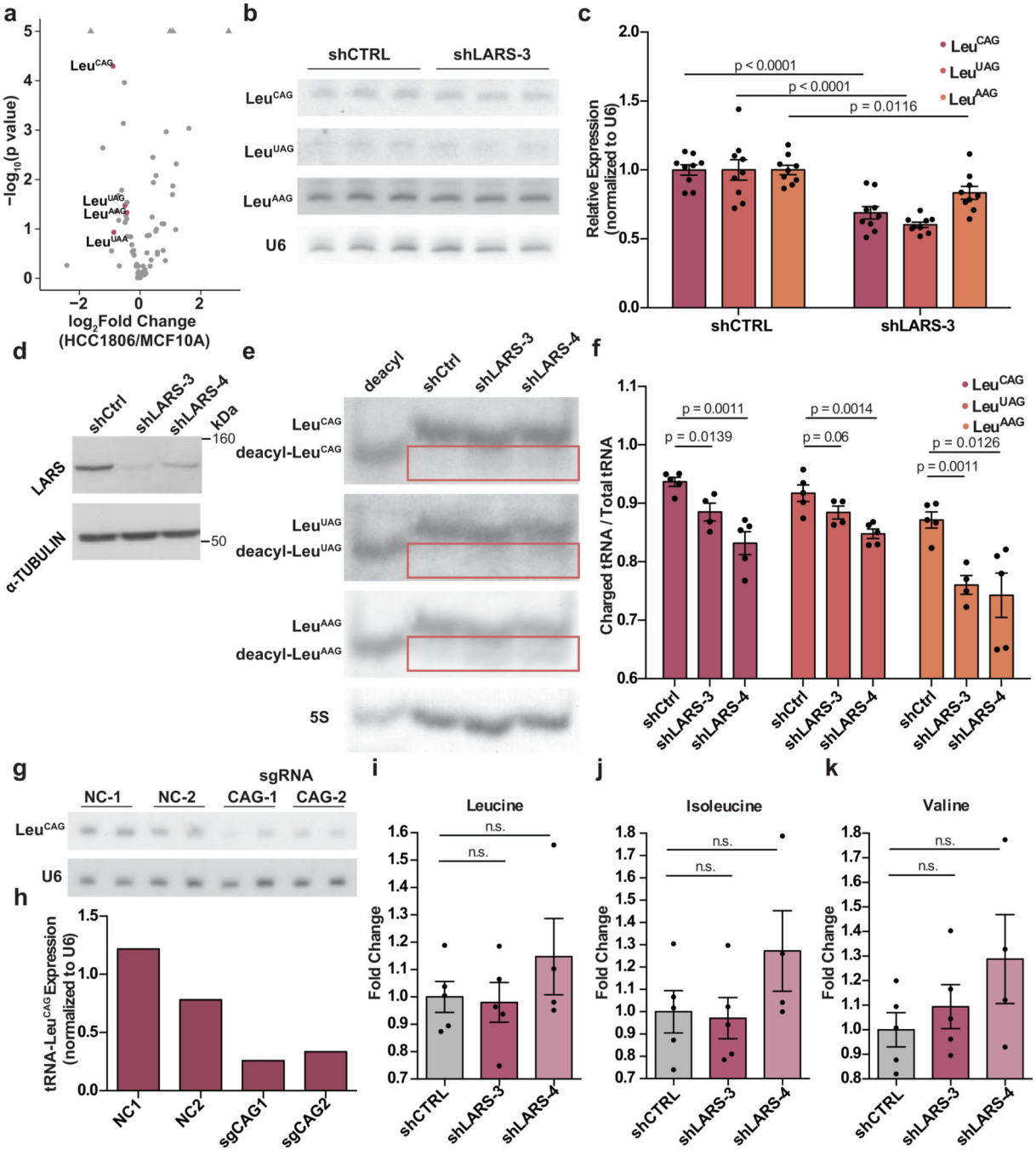

Extended Data Fig. 3. LARS reduction enhances tumorigenesis through depletion of tRNA-Leu^{CAG}.

a, Volcano plot showing differential expression of total tRNAs in HCC1806 cell line compared to MCF10A (n=3 per group). b, Northern blot validation of reduction in tRNA-Leu species in LARS-depleted 4T07 cells compared to control. c, Quantification of b, n=8–9 replicates examined over 3 independent experiments. Statistics calculated by unpaired two-tailed Student's t-test. d, Western blot depicting LARS knockdown levels in 4T07 cells with two independent shRNAs. Representative of n=3 independent experiments. e, Northern blot validation of reduction in charged tRNA-Leu species by acid urea PAGE in LARS-depleted 4T07 cells compared to control. Deacyl species are boxed for clarification. Representative of n=3 independent experiments. f, Quantification of e as a ratio of charged to total tRNA, n=4–5 replicates examined over 3 independent experiments. Statistics calculated by unpaired one-tailed Student's t-test. g, Northern blot depicting CRISPRi-mediated tRNA-Leu depletion in MCF10A cells. Representative of n=2 independent experiments. h, Quantification of g. i-k, In vivo metabolomics of branched chain amino acids in LARS-depleted 4T07 tumours (n=5 mice per group). n.s. by unpaired two-tailed Student's t-test. All data are mean ± s.e.m.

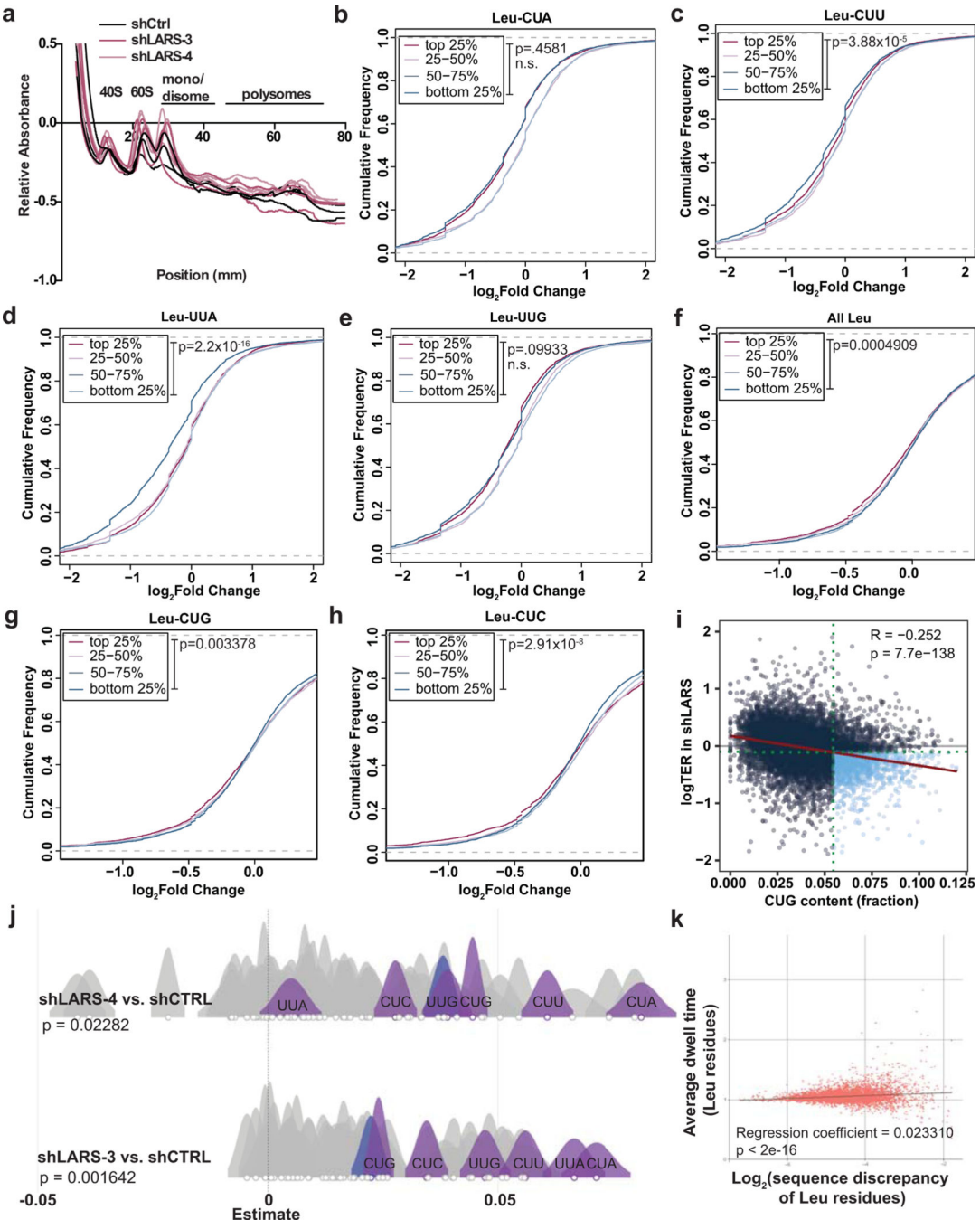

Extended Data Fig. 4. LARS facilitates Leu-rich translation for select isoacceptors *in vitro* and *in vivo*.

a, Polysome traces from gradient fractionation and polysome profiling in LARS-depleted 4T07 cells compared to control. (n=3 samples per group). b-e, Cumulative distribution functions of differentially expressed genes by polysome occupancy, stratified by Leu-CUA (b), Leu-CUU (c), Leu-UUA (d), and Leu-UUG (e) codon content, respectively. p < .4581 (b), p < 3.88e-5 (c), p < 2.20e-16 (d), p < 0.09933 (e), two-sided KS test. f-h, Cumulative distribution functions of differential gene expression by RiboTag (n=3 mice per group), stratified by abundance of Leu isoacceptors (f) Leu-CUG (g) and Leu-CUC (h). p =

0.0004909 (f), p < 0.003378 (g), p < 2.91e-8 (h), two-sided KS test. i, scatter plot of RiboSeq log2 fold translation efficiency ratios (logTER) in LARS depleted cells compared to control, plotted as a function of fractional CUG codon content (n=2 samples per group). Regression coefficient R = −0.252, p = 7.7 e-138. j, Ribosome dwell time analysis in RiboSeq data (n=2 samples per group). Leu codons show increased dwell time compared to other codons in Lars knockdown relative to control. shCtrl vs. shLars3, p = 0.001642; shCtrl vs. shLars4, p = 0.02282, Kruskal Wallis rank sum test. k, Analysis of Leucine sequence discrepancy, or “clumpiness” on ribosome dwell time in 4T07 shCtrl cells. Regression coefficient = 0.023310, p < 2e-16.

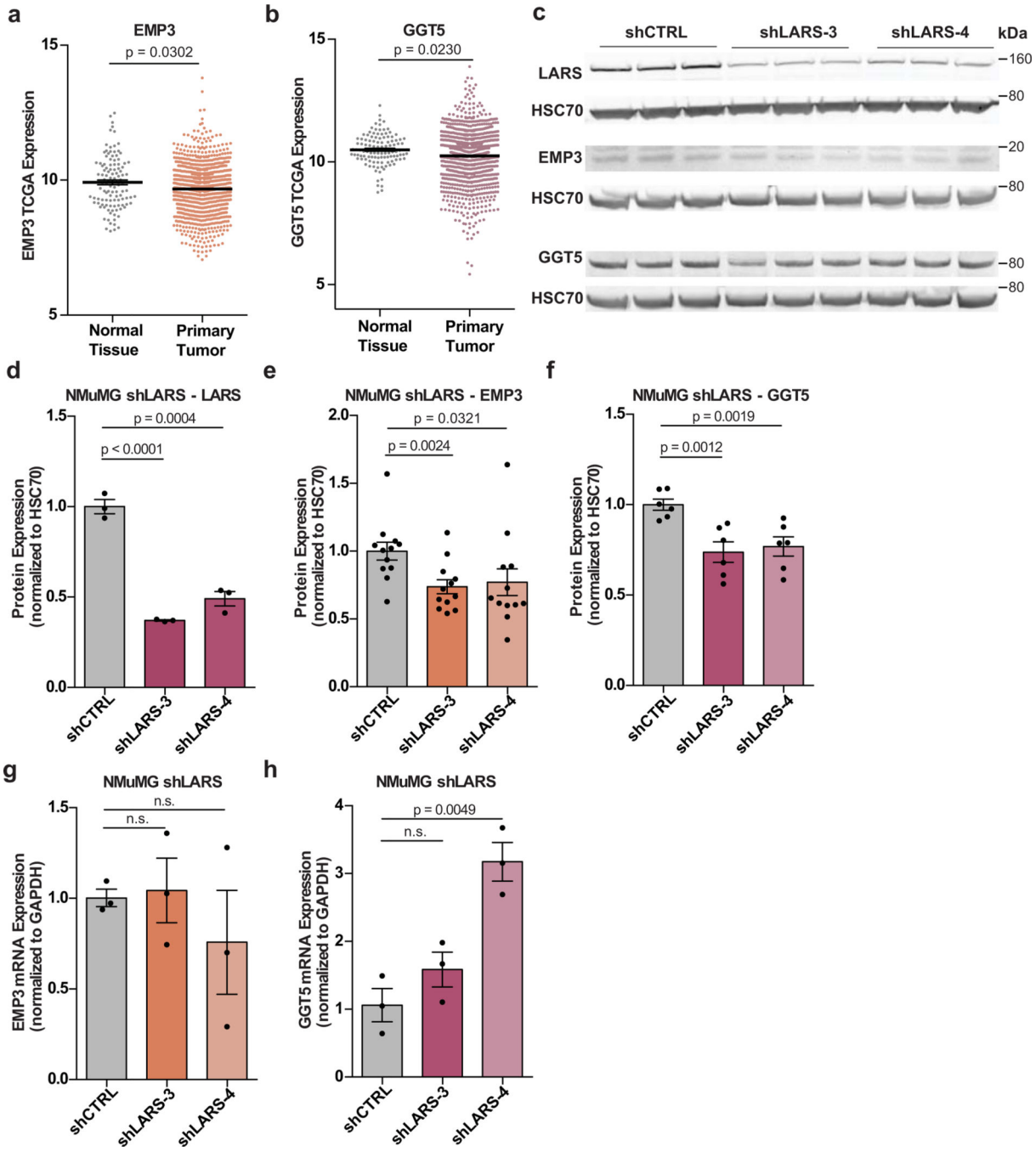

Extended Data Fig. 5. LARS regulates protein expression of tumor suppressors EMP3 and GGT5.

a,b, Clinical association of EMP3, GGT5 in the TCGA database normal breast tissue samples compared to primary tumor. Statistics calculated by two-tailed Mann-Whitney test. c, Western blot of LARS, EMP3, and GGT5 in LARS-depleted NMuMG cells. HSC70 is used as a loading control. d, Quantification of LARS (n=3) in c, representative of 3 independent experiments. e-f, Quantification of EMP3 (n=12, e) or GGT5 (n=9, f) replicates over n=3 independent experiments. g,h, mRNA levels of EMP3, GGT5 in Lars-depleted NMuMG cells normalized to GAPDH, by qRT-PCR. Representative of n=3 independent

experiments. d-h, Statistics calculated by unpaired two-tailed Student's t-test. All data are mean ± s.e.m.

Supplementary Material

Refer to Web version on PubMed Central for supplementary material.

ACKNOWLEDGMENTS

We thank members of the Tavazoie laboratory for thoughtful feedback on previous versions of the manuscript. We also thank The Rockefeller University resource centers: Connie Zhao and Christine Lai from the Genomics Resource Center, Alison North and staff at the Bio-Imaging resource facility, Vaughn Francis from the Comparative Bioscience Center and veterinary staff for animal husbandry and care. M.C.P was supported by a Medical Scientist Training Program grant from the National Institute of General Medical Sciences of the National Institutes of Health under award number T32GM007739 to the Weill Cornell/Rockefeller/Sloan Kettering Tri-Institutional MD-PhD program, and by an F30 Predoctoral Fellowship from the National Cancer Institute of the National Institutes of Health under award number 1F30CA247026-01. H.A. was supported by a training grant from the National Institutes of Health under award number F32GM133118. H.G. was supported by a R01 from the National Cancer Institute of the National Institutes of Health under award number R01CA240984. S.F.T. was supported by the Breast Cancer Research Foundation award, the Reem-Kayden award, the Department of Defense Collaborative Scholars and Innovators award, and a Faculty Scholars award from the Howard Hughes Medical Institute. S.F.T. and the Tavazoie lab were supported by the Black Family and the Black Family Metastasis Research Center. The results published here are in part based upon data generated by the TCGA Research Network: https://www.cancer.gov/tcga. Some figures were generated with assistance from biorender.com.

REFERENCES

1. Hanahan D & Weinberg RA Hallmarks of cancer: The next generation. Cell 144, 646–674 (2011). [PubMed: 21376230]
2. Ruggero D Translational control in cancer etiology. Cold Spring Harb. Perspect. Biol. 5, (2013).
3. Leprivier G, Rotblat B, Khan D, Jan E & Sorensen PH Stress-mediated translational control in cancer cells. Biochim. Biophys. Acta - Gene Regul. Mech. 1849, 845–860 (2015).
4. Loayza-Puch F et al. Tumour-specific proline vulnerability uncovered by differential ribosome codon reading. Nature 530, 490–494 (2016). [PubMed: 26878238]
5. Ebright RY et al. Deregulation of ribosomal protein expression and translation promotes breast cancer metastasis. Science (80-.). 367, 1468–1473 (2020).
6. Novoa EM & Ribas de Pouplana L Speeding with control: Codon usage, tRNAs, and ribosomes. Trends Genet. 28, 574–581 (2012). [PubMed: 22921354]
7. Knott SRV et al. Asparagine bioavailability governs metastasis in a model of breast cancer. Nature 554, 378–381 (2018). [PubMed: 29414946]
8. Goodarzi H et al. Modulated Expression of Specific tRNAs Drives Gene Expression and Cancer Progression. Cell 165, 1416–1427 (2016). [PubMed: 27259150]
9. Pavon-Eternod M et al. tRNA over-expression in breast cancer and functional consequences. Nucleic Acids Res. 37, 7268–7280 (2009). [PubMed: 19783824]
10. Kirchner S & Ignatova Z Emerging roles of tRNA in adaptive translation, signalling dynamics and disease. Nat. Rev. Genet. 16, 98–112 (2014). [PubMed: 25534324]
11. Zhang Z et al. Global analysis of tRNA and translation factor expression reveals a dynamic landscape of translational regulation in human cancers. Commun. Biol. 1, 1–11 (2018). [PubMed: 29809203]
12. Zhou Z, Sun B, Nie A, Yu D & Bian M Roles of Aminoacyl-tRNA Synthetases in Cancer. Front. Cell Dev. Biol. 8, 1–12 (2020). [PubMed: 32117956]
13. Park SG, Schimmel P & Kim S Aminoacyl tRNA Synthetases and Their Connections To Disease. 105, 11043–11049 (2008).
14. Vo M-N et al. ANKRD16 prevents neuron loss caused by an editing-defective tRNA synthetase. Nature 557, 510–515 (2018). [PubMed: 29769718]

15. Antonellis A et al. Glycyl tRNA synthetase mutations in Charcot-Marie-Tooth disease type 2D and distal spinal muscular atrophy type V. Am. J. Hum. Genet. 72, 1293–1299 (2003). [PubMed: 12690580]
16. Komarov PG et al. A Chemical Inhibitor of p53 That Protects Mice from the Side Effects of Cancer Therapy. Science (80-.). 285, 1733 LP–1737 (1999).
17. Guy CT, Cardiff RD & Muller WJ Induction of Mammary Tumors by Expression of Polyomavirus Middle T Oncogene : A Transgenic Mouse Model for Metastatic Disease. Mol. Cell. Biol. 12, 954–961 (1992). [PubMed: 1312220]
18. Testa G et al. A Reliable lacZ Expression Reporter Cassette for Multipurpose, Knockout-First Alleles. Genesis 38, 151–158 (2004). [PubMed: 15048813]
19. Tavora B et al. Tumoural activation of TLR3–SLIT2 axis in endothelium drives metastasis. Nature 586, 299–304 (2020). [PubMed: 32999457]
20. Padmanaban V et al. Organotypic culture assays for murine and human primary and metastatic-site tumors. Nat. Protoc. 15, 2413–2442 (2020). [PubMed: 32690957]
21. Han JM et al. Leucyl-tRNA synthetase is an intracellular leucine sensor for the mTORC1-signaling pathway. Cell 149, 410–424 (2012). [PubMed: 22424946]
22. He X. Di et al. Sensing and Transmitting Intracellular Amino Acid Signals through Reversible Lysine Aminoacylations. Cell Metab. 27, 151–166.e6 (2018). [PubMed: 29198988]
23. Pavlova NN et al. Translation in amino-acid-poor environments is limited by tRNA Gln charging. Elife 1–27 (2020) doi:10.7554/eLife.62307.
24. Gobet C et al. Robust landscapes of ribosome dwell times and aminoacyl-tRNAs in response to nutrient stress in liver. PNAS 1–12 (2020) doi:10.1073/pnas.1918145117.
25. Evans ME, Clark WC, Zheng G & Pan T Determination of tRNA aminoacylation levels by high-throughput sequencing. Nucleic Acids Res. 45, e133 (2017). [PubMed: 28586482]
26. Lund Elsebet, Dahlberg JE Proofreading and Aminoacylation of tRNAs before Export from the Nucleus. Science (80-.). 282, 2082–2085 (1998).
27. Elf J, Nilsson D, Tenson T & Ehrenberg M Selective charging of tRNA isoacceptors explains patterns of codon usage. Science (80-.). 300, 1718–1722 (2003).
28. Gilbert LA et al. Genome-Scale CRISPR-Mediated Control of Gene Repression and Activation Luke. 159, 647–661 (2014).
29. Chan PP & Lowe TM GtRNAdb: A database of transfer RNA genes detected in genomic sequence. Nucleic Acids Res. 37, 93–97 (2009).
30. Chan PP & Lowe TM GtRNAdb 2.0: An expanded database of transfer RNA genes identified in complete and draft genomes. Nucleic Acids Res. 44, D184–D189 (2016). [PubMed: 26673694]
31. Novoa EM, Pavon-Eternod M, Pan T & Ribas De Pouplana L A role for tRNA modifications in genome structure and codon usage. Cell 149, 202–213 (2012). [PubMed: 22464330]
32. Sanz E et al. Cell-type-specific isolation of ribosome-associated mRNA from complex tissues. Proc. Natl. Acad. Sci. 106, 13939–13944 (2009).
33. McGlincy NJ & Ingolia NT Transcriptome-wide measurement of translation by ribosome profiling. Methods 126, 112–129 (2017). [PubMed: 28579404]
34. Zecha J et al. TMT labeling for the masses: A robust and cost-efficient, in-solution labeling approach. Mol. Cell. Proteomics 18, 1468–1478 (2019). [PubMed: 30967486]
35. Wang YW, Cheng HL, Ding YR, Chou LH & Chow NH EMP1, EMP 2, and EMP3 as novel therapeutic targets in human cancer. Biochim. Biophys. Acta - Rev. Cancer 1868, 199–211 (2017). [PubMed: 28408326]
36. Alaminos M et al. EMP3, a myelin-related gene located in the critical 19q13.3 region, is epigenetically silenced and exhibits features of a candidate tumor suppressor in glioma and neuroblastoma. Cancer Res. 65, 2565–2571 (2005). [PubMed: 15805250]
37. Wang W et al. Effector T Cells Abrogate Stroma-Mediated Chemoresistance in Ovarian Cancer. Cell 165, 1092–1105 (2016). [PubMed: 27133165]
38. Xu Y et al. Translation control of the immune checkpoint in cancer and its therapeutic targeting. Nat. Med. 25, 301–311 (2019). [PubMed: 30643286]

39. Dittmar KA, Sørensen MA, Elf J, Ehrenberg M & Pan T Selective charging of tRNA isoacceptors induced by amino-acid starvation. EMBO Rep. 6, 151–157 (2005). [PubMed: 15678157]
40. Darnell AM, Subramaniam AR & O'Shea EK Translational Control through Differential Ribosome Pausing during Amino Acid Limitation in Mammalian Cells. Mol. Cell 71, 229–243.e11 (2018). [PubMed: 30029003]
41. Huh D et al. A stress-induced tyrosine-tRNA depletion response mediates codon-based translational repression and growth suppression. EMBO J. 40, 1–16 (2021).
42. Shin S-H et al. Implication of leucyl-tRNA synthetase 1 (LARS1) over-expression in growth and migration of lung cancer cells detected by siRNA targeted knock-down analysis. Exp. Mol. Med. 40, 229–236 (2008). [PubMed: 18446061]
43. Gomez MAR & Ibba M Aminoacyl-tRNA Synthetases. RNA 26, 910–936 (2020). [PubMed: 32303649]
44. Perona JJ & Hou Y-M Indirect Readout of tRNA for Aminoacylation. Biochemistry 46, 10419–10432 (2007).
45. Tocchini-Valentini G, Saks ME & Abelson J tRNA leucine identity and recognition sets. J. Mol. Biol. 298, 779–793 (2000). [PubMed: 10801348]
46. Park SJ & Schimmel P Evidence for interaction of an aminoacyl transfer RNA synthetase with a region important for the identity of its cognate transfer RNA. J. Biol. Chem. 263, 16527–16530 (1988). [PubMed: 3053691]
47. Fender A, Sissler M, Florentz C & Giegé R Functional idiosyncrasies of tRNA isoacceptors in cognate and noncognate aminoacylation systems. Biochimie 86, 21–29 (2004). [PubMed: 14987797]
48. McFarland MR et al. The molecular aetiology of tRNA synthetase depletion: induction of a GCN4 amino acid starvation response despite homeostatic maintenance of charged tRNA levels. Nucleic Acids Res. 48, 3071–3088 (2020). [PubMed: 32016368]
49. Guo M & Schimmel P Essential nontranslational functions of tRNA synthetases. Nat. Chem. Biol. 9, 145–153 (2013). [PubMed: 23416400]

ADDITIONAL METHOD REFERENCES

50. Gandin V et al. Polysome fractionation and analysis of mammalian translatomes on a genome-wide scale. J. Vis. Exp. 1–9 (2014) doi:10.3791/51455.
51. Xiao Z, Zou Q, Liu Y & Yang X Genome-wide assessment of differential translations with ribosome profiling data. Nat. Commun. 7, (2016).
52. Lauria F et al. riboWaltz: Optimization of ribosome P-site positioning in ribosome profiling data. PLoS Comput. Biol. 14, 1–20 (2018).
53. Hickernell FJ Quadrature Error Bound. Math. Comput. 67, 299–322 (1998).
54. Tyanova S et al. The Perseus computational platform for comprehensive analysis of (prote)omics data. Nat. Methods 13, 731–740 (2016). [PubMed: 27348712]
55. Wagner KU et al. Cre-mediated gene deletion in the mammary gland. Nucleic Acids Res. 25, 4323–4330 (1997). [PubMed: 9336464]

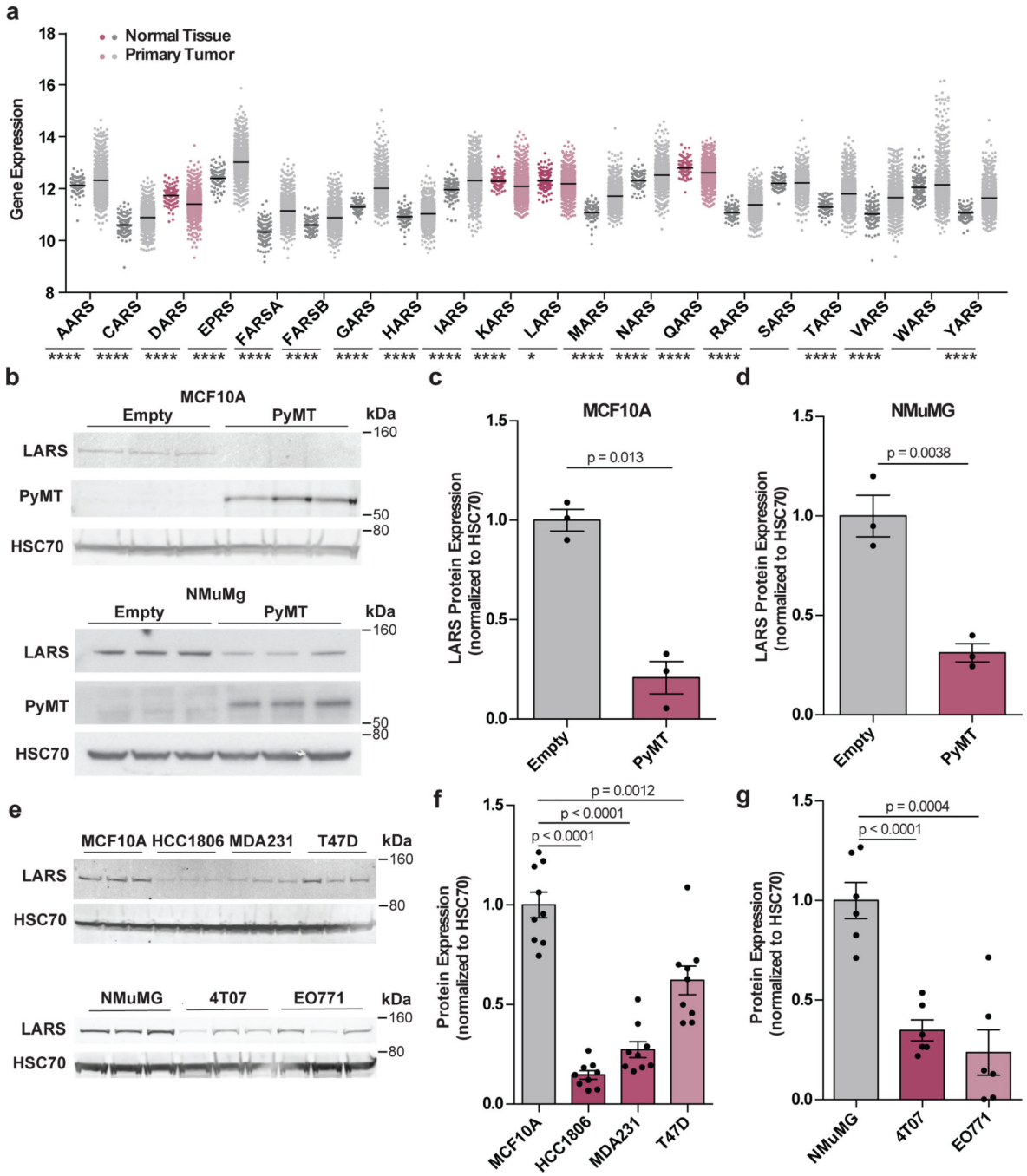

Figure 1. Clinical evidence of LARS reduction upon malignant transformation.

a, Aminoacyl tRNA synthetase (aaRS) expression levels in the TCGA database in normal breast tissue samples (dark gray or magenta) compared to primary tumor samples (light gray or pink). Magenta and pink-colored expression pairs indicate significant reduction in expression in primary tumor samples compared to normal breast tissue. Statistics measured by two-tailed KS test with Bonferroni's correction and indicated with stars below the X axis. * p = 0.042, **** = p<0.001. **b,** Western blot of LARS protein levels in transformed MCF10A (above) and NMuMG (below) cells. Transformation is indicated

by PyMT expression, HSC70 is used as a loading control. **c,d,** Quantification of **b**. Representative of n=3 independent experiments. **e**, Above, Western blot of LARS protein levels in non-transformed human mammary epithelial cell line MCF10A, triple negative HCC1806, MDA-MB-231 and ER-positive T47D cell lines. Below, LARS protein levels in non-transformed murine mammary epithelial line NMuMg, and murine breast tumor lines 4T07 and EO771. HSC70 is used as a loading control. **f,g,** Quantification of n=9 (**f**) or n=6 (**g**) biological replicates examined over 3 independent experiments in **e**. Blots are representative of n=3 independent experiments. **b-g**, Data are mean ± s.e.m. Statistics calculated by unpaired two-tailed Student's t-test.

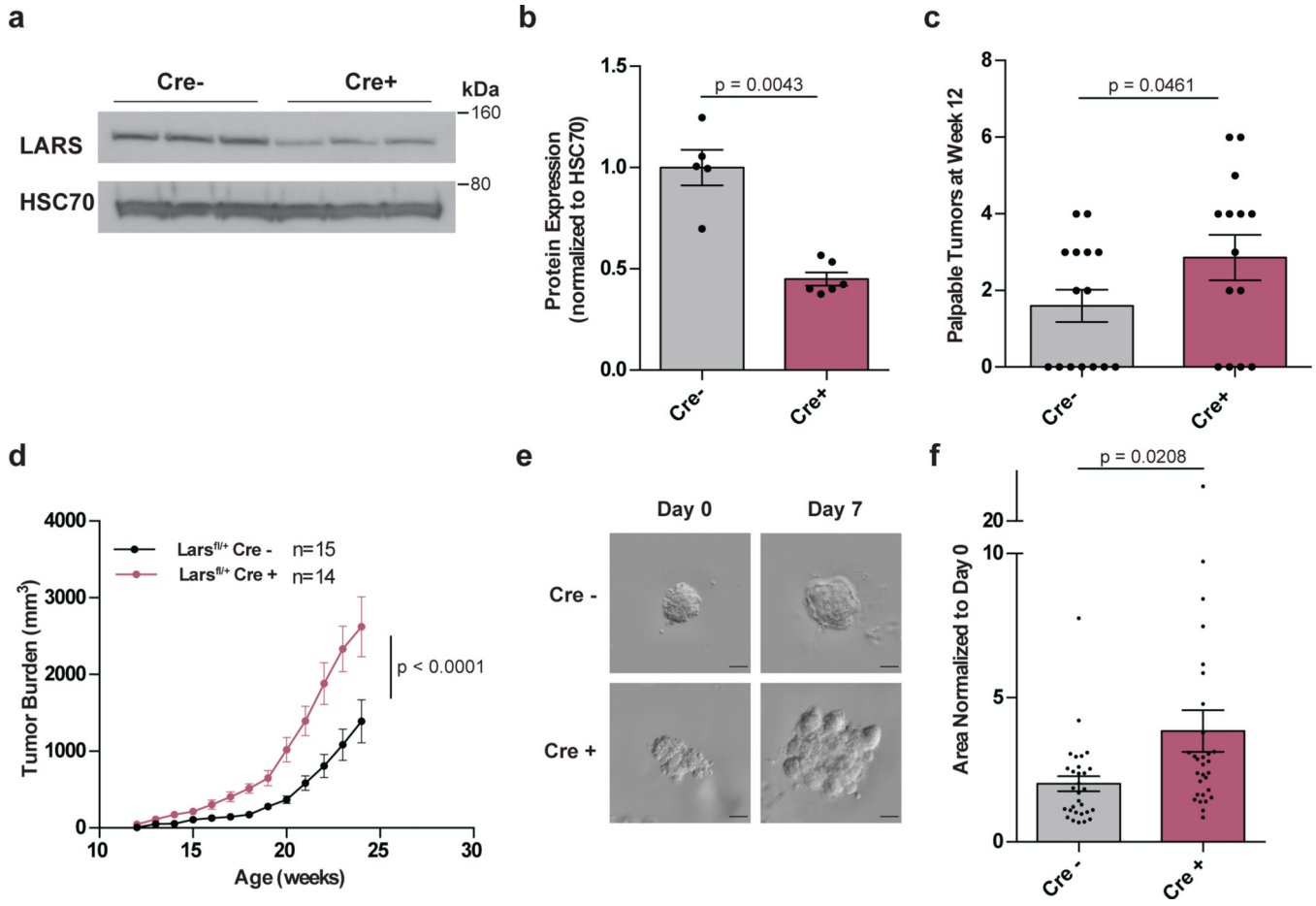

Figure 2. LARS suppresses tumourigenesis and proliferation.

a, Western blot of LARS levels in MMTV-*Cre*-expressing PyMT tumours with monoallelic LARS deletion compared to *Cre*-negative animals. *Cre* expression results in 50% reduction in protein levels. Representative of n=5 (Cre-) or n=6 (Cre+) replicates examined over n=3 independent blots, each replicate is from one mouse tumor. **b,** Quantification of **a**. Statistics calculated by unpaired two-tailed Student's t-test. **c,** Number of palpable initiated tumours per mouse at week 12 in PyMT model with LARS deletion. *Cre+* n=14, *Cre-* n=15, statistics calculated by unpaired one-tailed Student's t- test. **d,** Growth curves depicting overall tumour burden in PyMT model animals stratified by MMTV-*Cre* expression. *Cre+* n=14, *Cre-* n=15, Statistics calculated by 2-way ANOVA. **e,** Representative images of LARS-depleted PyMT tumour-derived organoids cultured in Matrigel. Scale bar, 100 μm. **f**, Quantification of change in 2D projection of organoid area, normalized to Day 1. n=30 organoids examined per experimental group, representative of 3 independent experiments. Statistics calculated by unpaired two-tailed Student's t-test. All data are mean ± s.e.m.

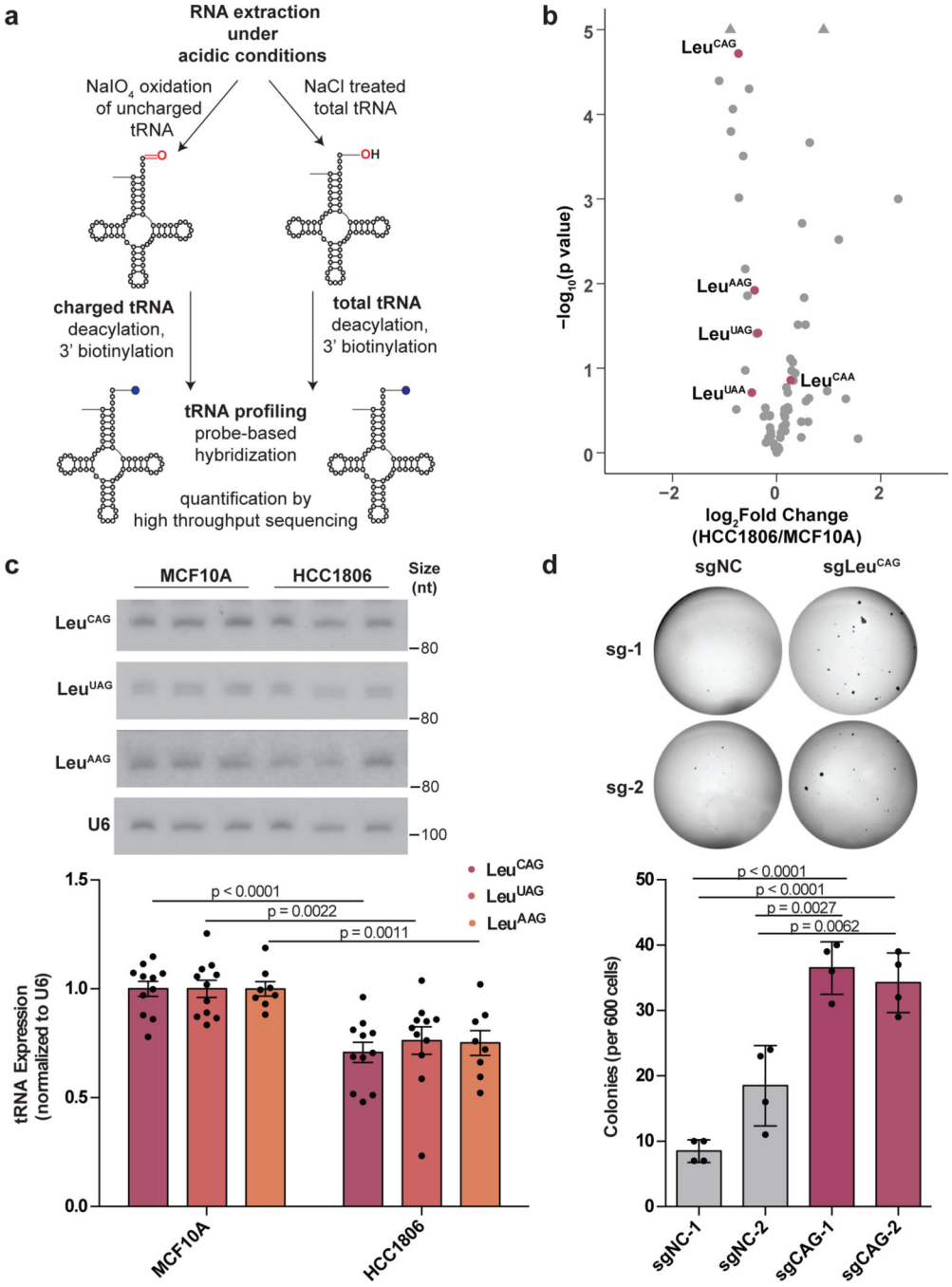

Figure 3. Charged tRNA profiling reveals reduction in select tRNA-Leu isoacceptors.

a, Experimental overview of charged tRNA profiling. **b,** Volcano plot showing differential expression of charged tRNAs in HCC1806 cell line compared to MCF10A (n=3 samples per group). **c,** Northern blot validation of reduction in tRNA-Leu species in HCC1806 compared to MCF10A, quantified below as n=11 (tRNA-Leu^{CAG} and tRNA-Leu^{AAG}) or n=8 (tRNA-Leu^{TAG}) replicates examined over 3 independent experiments. Blot is representative of n=3 independent experiments. **d,** Representative colony formation assays of PyMT-transformed, tRNA-Leu^{CAG} depleted MCF10A cells, quantified below, n=4

replicates per group, representative of n=3 independent experiments. Statistics calculated by unpaired two-tailed Student's t-test. All data are mean ± s.e.m.

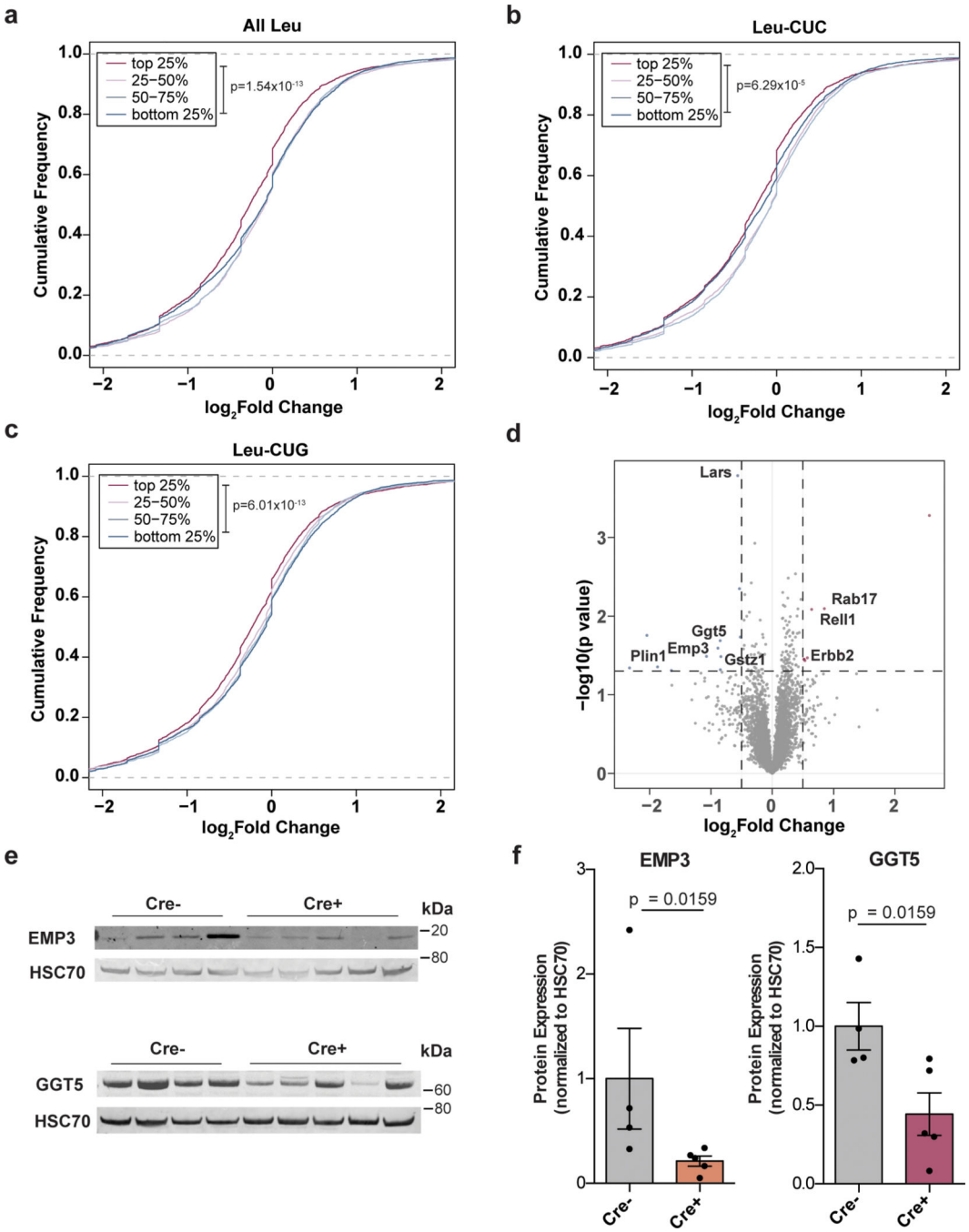

Figure 4. LARS promotes translation and expression of Leu-enriched genes.

a, Cumulative distribution functions of differentially expressed genes by polysome occupancy, stratified by overall Leu codon content. Genes with higher Leu codon content have relatively left-shifted $\log_2$ fold changes, indicating lower translation in Lars knockdown (n=3 samples per group). **b,c,** as in **a**, stratified by individual Leu-CUC and Leu-CUG isoacceptor content, respectively. p < 1.54e-13 (**a**), p < 6.01e-13 (**b**), p < 6.29e-5 (**c**), two-sided KS test. **d,** Volcano plot of differentially detected proteins in TMT-labeled proteomics in PyMT Lars knockout tumours compared to control. Cutoffs of $\log_2$ fold change < |0.5|

and $p < 0.05$ (unpaired two-tailed Student's t-test) indicated by dotted lines (n=5 tumors per group). **e,** Western blot expression of candidate downstream targets EMP3 and GGT5 in LARS-depleted PyMT tumours. HSC70 is used as a loading control. Samples represent individual mice *Cre-* n=4, *Cre+* n=5. **f,** Quantification of **e**. Statistics calculated by one-tailed Mann-Whitney test. Data are mean ± s.e.m.

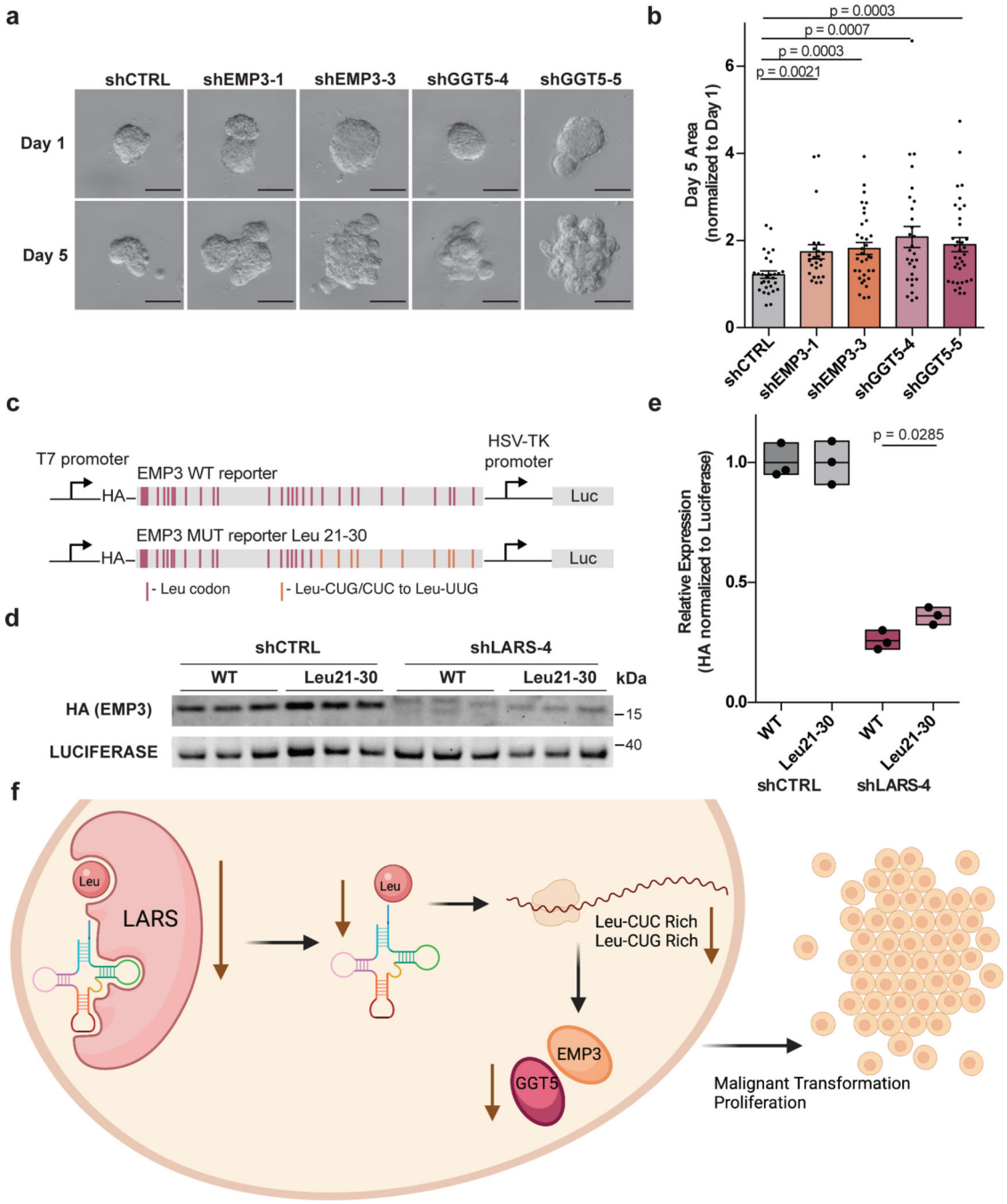

Figure 5. EMP3 and GGT5 regulate growth downstream of LARS in a codon-dependent manner.

a, Representative images of wild-type MMTV-PyMT tumor-derived organoids with shRNA knockdown of EMP3 and GGT5, cultured in 3D Matrigel. Scale bar, 100 μm. **b,** Quantification of change in 2D projection of organoid area, normalized to Day 1. 25–35 organoids quantified per experimental group, representative of n=3 experiments. **c,** Schematic overview of EMP3 codon reporter design. For leucine codons 21–30 in the gene, Leu-CUC and Leu-CUG codons were replaced with Leu-TTG codons. **d,** Western blot for EMP3 reporter expression (HA expression) in NMuMG LARS depleted cell lines.

Luciferase is used as a transfection control. Representative of n=4 independent experiments. **e,** quantification of **d**. Bounds of boxes represent minimum and maximum values, center line represents mean value. Statistics calculated by unpaired two-tailed Student's t-test, all data are mean ± s.e.m. **f,** Model of LARS-mediated suppression of tumourigenesis.